Title

Origins of choice-related activity in mouse somatosensory cortex

Journal

Nature Neuroscience, 19(1)

ISSN

1097-6256

Authors

Yang, Hongdian

Kwon, Sung E

Severson, Kyle S

et al.

Publication Date

2016

DOI

10.1038/nn.4183

Peer reviewed

HHS Public Access

Author manuscript

Nat Neurosci. Author manuscript; available in PMC 2016 June 07.

Published in final edited form as:

Nat Neurosci. 2016 January ; 19(1): 127–134. doi:10.1038/nn.4183.

Origins of choice-related activity in mouse somatosensory cortex

Hongdian Yang[*], **Sung E. Kwon**[*], **Kyle S. Severson**, and **Daniel H. O'Connor**

The Solomon H. Snyder Department of Neuroscience & Brain Science Institute, The Johns Hopkins University School of Medicine, Baltimore, MD 21205

Abstract

During perceptual decisions about faint or ambiguous sensory stimuli, even identical stimuli can produce different choices. Spike trains from sensory cortex neurons can predict trial-to-trial variability in choice. Choice-related spiking is widely studied to link cortical activity to perception, but its origins remain unclear. Using imaging and electrophysiology, we found that mouse primary somatosensory cortex neurons showed robust choice-related activity during a tactile detection task. Spike trains from primary mechanoreceptive neurons did not predict choices about identical stimuli. Spike trains from thalamic relay neurons showed highly transient, weak choice-related activity. Intracellular recordings in cortex revealed a prolonged choice-related depolarization in most neurons that was not accounted for by feedforward thalamic input. Top-down axons projecting from secondary to primary somatosensory cortex signaled choice. An intracellular measure of stimulus sensitivity determined which neurons converted choice-related depolarization into spiking. Our results reveal how choice-related spiking emerges across neural circuits and within single neurons.

Introduction

For decades it has been known that the spike trains of sensory cortex neurons can predict trial-to-trial variability in perceptual decisions about identical stimuli[1–3]. Correlations between sensory neuron spike trains and behavioral choices are often quantified using "choice probability"[1] or "detect probability"[4,5], the probability with which an ideal observer could predict behavioral choice based on neural activity evoked by identical stimuli. Choice-related activity (choice or detect probability > 0.5) has been observed in multiple sensory brain areas, including monkey extrastriate[1,2,4,6–10] and primary[11,12] visual cortex, monkey

Correspondence and requests for materials should be addressed to ; Email: dan.oconnor@jhmi.edu

*These authors contributed equally to this work

Author Contributions

HY, SK and DO planned the project. HY, SK and KS performed experiments. HY and DO built apparatus. All authors analyzed data. HY, SK and DO wrote the paper with comments from KS.

Author Information

The authors declare no competing financial interests.

A Supplementary Methods Checklist is available.

vestibular and cerebellar nuclei[6], monkey somatosensory cortex[13,14], and rodent olfactory bulb[15].

Correlated trial-to-trial variability between spike trains and choice has been widely studied in order to link cortical activity to perception[1,2,4,6–9,11–15]. However, interpreting these correlations requires understanding the underlying sources of variability. Choice-related variability in cortical spiking could reflect variability in the primary sensory afferents[16], could accumulate in a feedforward manner[17] as activity propagates from the sensory periphery to cortex, or could reflect non-stimulus-driven, "top-down" influences on sensory cortex[8]. The contributions of these and other sources of variability to cortical responses remain poorly understood.

To address this problem, we developed a preparation to study choice-related activity during tactile detection in mice. We recorded from the primary mechanoreceptor afferent neurons that transduce tactile stimuli into action potentials, from thalamus neurons that provide the main feedforward drive to cortex, and from primary somatosensory (S1, barrel) cortex neurons. Choice-related variability in spike rate was absent in the primary afferents, and was weak and transient in thalamic relay neurons. Intracellular recordings in cortex showed a prolonged choice-related depolarization in most neurons. Choice-related activity was present in top-down axons projecting from secondary somatosensory cortex to S1. An intracellular measure of stimulus sensitivity (the touch reversal potential[18–21]) determined which neurons converted choice-related depolarization into choice-related spiking.

Results

We trained mice in a simple head-fixed, Go/NoGo tactile detection task (Fig. 1a,b). Each trial began with an auditory cue to alert the mice to the time of possible stimulus onset (Fig. 1b). This cue was intended to eliminate ambiguity about the time at which the stimulus could arrive. A single whisker was deflected with a sinusoidal waveform (0.5 s, 20 or 40 Hz; Methods) on 50% of trials (Go trials). On the other 50% of trials, the whisker was not deflected. Lick responses occurring during a response window (Fig. 1b) determined trial outcome (Fig. 1c). Task performance varied with the strength (angular speed) of the whisker stimulus (Fig. 1d). Spiking responses increased monotonically for these whisker stimuli in the primary afferents, thalamus, and S1 (Supplementary Fig. 1a). When we randomly interleaved trials with stimulation of three whiskers rather than one whisker, performance increased even as the single-whisker curve began to saturate (Fig. 1d). Thus, tasks performed with a single whisker may be perceptually demanding for mice, even with relatively strong stimulation (cf. [19,22,23]). Strong multi-whisker stimulation led to high performance (~85% correct), indicating that performance was limited by the stimulus rather than task engagement (Fig. 1d). For subsequent experiments, we used a stimulus strength (single whisker, ~500–900 degrees/s; cf. [24]) that yielded a mixture of detection successes (Hits) and failures (Misses). Performance with this stimulus strength resulted in performance of ~70% correct even after several weeks of training (Supplementary Fig. 1d).We analyzed Hit, Miss and Correct Rejection trials (Fig. 1c), over periods prior to the typical reaction times (Supplementary Fig. 1). Because whisking produces self-generated tactile input that can affect detection behavior[25], we limited analysis to periods of passive stimulation (Methods).

Performance was abolished by reversibly silencing somatosensory cortex using optogenetic stimulation of GABAergic neurons[19,22,23] (Supplementary Fig. 2).

Choice-related activity in mouse somatosensory cortex

We used two-photon calcium imaging to record spiking-related activity[26] of cortical layer 2/3 neurons in S1, in the C2-whisker and surrounding columns (Fig. 1e). Correct Rejection trials (with no stimulus applied) showed no evoked activity (Fig. 1f,g). Hit trials and Miss trials (with identical C2 whisker stimuli applied) each showed robust evoked activity, but evoked responses were larger on Hit compared with Miss trials (Fig. 1f,g; 0.018 ± 0.002 vs 0.013 ± 0.002 $\Delta F/F_0$, K-S test, $p < 1e{-}3$, n = 1,746 neurons in 6 mice). Thus, S1 responses for the same stimulus predict perceptual choice.

No choice-related spiking in primary afferent neurons

We sought to trace the origins of the choice-related activity we observed in primary somatosensory cortex. We began at the earliest possible stage: the primary mechanoreceptive afferents that transduce mechanical stimuli into action potentials. These neurons innervate the whisker follicle, have cell bodies located in the trigeminal ganglion, and send projections to somatosensory brainstem nuclei. Trigeminal ganglion neurons have single-whisker receptive fields[27]. We made extracellular recordings from single trigeminal ganglion neurons while mice performed the detection task using the single whisker in the neuron's receptive field (Fig. 2). We analyzed spike rates during a baseline period, prior to the time of possible stimulus onset, and during a window shortly after the stimulus onset but prior to the typical reaction time on Go trials. Trigeminal ganglion neurons had low baseline spike rates that did not differ between Hit and Miss trials (0.77 ± 20.1 vs 0.62 ± 28.4 Hz [median ± interquartile range], p = 0.55, two-tailed sign test, n = 17; Fig. 2c,e), indicating that pre-stimulus activity in primary afferents was not a significant factor in perceptual outcome. Neurons were strongly driven by the whisker stimulus during both Hit and Miss trials (Fig. 2b,c). There was no difference in evoked rate between the two trial types (82.5 ± 9.2 vs 79.2 ± 9.9 Hz, p = 0.38; Fig. 2c,d).

Choice probability[1] is the probability with which an ideal observer could predict the choice of the animal (here corresponding to a Hit or a Miss), given the neural response. In the context of detection tasks, the same quantity is often referred to as "detect probability" (DP)[4,5]; we adopt this convention here. We asked how well an ideal observer could predict the choice of the animal given the trigeminal ganglion spike trains. We also calculated "stimulus probability" (SP, Methods), which is calculated similarly but quantifies how well an ideal observer could categorize the sensory stimulus (in our case, stimulus presence vs absence) based on the neural response. Trigeminal ganglion neurons robustly signaled the presence or absence of the stimulus (SP calculated over the "evoked" window: 0.94 ± 0.02, $p < 1e{-}3$, two-tailed sign test of SP = 0.5, Methods; shown calculated in a moving window: Fig. 2f gray trace), but not the subsequent perceptual choice of the animal (DP over the evoked window: 0.52 ± 0.02, p = 0.41; shown in a moving window: Fig. 2f, black trace).

Transient, weak choice-related spiking in thalamus

Choice-related activity was present in primary somatosensory cortex (Fig. 1), but not in the primary mechanoreceptive afferents (Fig. 2). Does choice-related activity emerge en route to cortex? Whisker touch information arrives to cortex largely along thalamocortical axons from the ventral posteromedial nucleus of thalamus (VPM). We recorded extracellular multiunit spiking activity (MUA, typically ~2–5 neurons) from regions of VPM that represent the whisker used to solve the detection task (Fig. 3a,b; Supplementary Fig. 3).

Baseline VPM spike rate was similar for Hits and Misses (20.0 ± 2.6 vs 18.7 ± 2.6 Hz, p = 0.14, two-tailed sign test, n = 17; Fig. 3c,f), indicating that at the thalamic level, pre-stimulus spike rate was not a critical determinant of perceptual choice. On Hit and Miss trials, thalamic activity increased rapidly following stimulus onset (latency from onset of whisker stimulation: 5–6 ms) and peaked early (~10–12 ms). VPM activity showed dramatic adaptation during the stimulus (Fig. 3c)[28]. Spike rates on Hit trials were slightly larger than on Misses, but only during a transient (~10 ms) window around the peak of the response (162.7 ± 21.0 vs 125.2 ± 26.0 Hz, p = 0.0065; Fig. 3c,d). This transient difference was also apparent in a measure of thalamic synchrony[29,30] (Supplementary Fig. 3). Shortly after the peak response, spike rates on Hits and Misses were no longer different (51.4 ± 7.5 vs 50.1 ± 7.7 Hz, measured in a 100 ms window starting 15 ms after stimulus onset, p = 0.63, two-tailed sign test; Fig. 3e). Spike rates on Hits and Misses did not differ during any other period in the trial (we did not analyze periods after the typical reaction time).

To quantify the ability of an ideal observer to predict the mouse's choice and the stimulus from VPM activity, we calculated detect probability and stimulus probability (Fig. 3g). Detect probability measured using spike rate over a brief window at the peak of the response (from 5–14 ms after stimulus onset) was significantly above chance (0.6 ± 0.03, p = 0.0086). This choice-related activity was fleeting, and disappeared immediately after the first peak in stimulus-evoked activity (mean DP from 15–114 ms after stimulus onset: 0.51 ± 0.03, p = 0.59). Stimulus probability peaked early (at peak: 0.85 ± 0.03, p < 1e–3), but remained above chance for the duration of the stimulus (not shown). Thus, VPM shows a weak, highly transient difference in stimulus-evoked spike rate that predicts choice.

What is the cortical impact of this transient, choice-related difference in thalamic spiking? First, we optogenetically approximated the spiking obtained on Hit and Miss trials (Fig. 3) by implanting an "optrode" in VPM of mice expressing channelrhodopsin-2 in VPM (Fig. 4 a–f; Methods). We paired whisker deflection with VPM photostimulation at a brief delay (0–4 ms from onset of whisker deflection), using either "weak" or "strong" light stimuli (a single 1 ms pulse, ~50 or 200 μW out of 105 μm optical fiber, respectively; exciting ~1–3 thalamic "barreloids"; Methods). Both strong and weak photostimulation led to a transient (< 15 ms) increase in VPM spike rate near the peak of the whisker-evoked response (whisker-alone vs whisker+light, weak light: 288.6 ± 32.7 vs 345.8 ± 38.2 Hz, p = 0.039, two-tailed sign test, n = 12; strong light: 270.2 ± 33.8 vs 391.7 ± 63.1 Hz, p = 0.039, two-tailed sign test, n = 9; Fig. 4 c,d). Spike rates in a window immediately after the peak of the whisker-evoked response were identical (whisker-alone vs whisker+light, weak light: 82.5 ± 10.3 vs 78.5 ± 9.7 Hz, p = 0.57, n = 12; strong light: 79.0 ± 13.7 vs 83.9 ± 16.6 Hz, p = 1.0, two-tailed sign test, n = 9; Fig. 4e). Thus, photostimulation approximated the transient

difference in thalamic spiking we observed previously between Hits and Misses (cf. Fig. 3c and Fig. 4c).

Next, we performed single-unit (loose-seal cell-attached[31]) recordings in the somatotopically aligned region of S1 (in the cortical column representing both the whisker used to solve the task and the stimulated region of VPM; Methods) while mice with an optrode in VPM performed the detection task (Fig. 4 g–m). Photostimulation in VPM led to a brief increase in S1 spike rate (whisker-alone vs whisker+light: weak light: 15.1 ± 5.8 vs 22.9 ± 8.1 Hz, p = 0.61, two-tailed sign test, n = 15; strong light: 15.1 ± 5.8 vs 57.2 ± 11.8 Hz, p < 1e–3, n = 15; Fig. 4i,j). The increase in S1 spiking was brief (~30 ms), even with strong photostimulation (in a window immediately after the peak whisker-evoked response: whisker-alone vs whisker+light, weak light: 9.7 ± 3.7 vs 9.1 ± 3.9 Hz, p = 0.54, n = 15; strong light: 9.7 ± 3.7 vs 2.6 ± 4.8 Hz, p = 0.42, two-tailed sign test, n = 15; Fig. 4k; see Supplementary Fig. 4 for related results in mice that were not task-engaged). For strong but not weak photostimulation, the increase in spiking was followed by a trend toward modest inhibition (Fig. 4k). Strong stimulation produced a decrease in Hit rate (Fig. 4m). A decreased Hit rate in the presence of late inhibition is consistent with a finding that the late cortical response to whisker deflection determines behavioral detection[19].

Together, our photostimulation experiments show that a transient increase in thalamic relay neuron spiking, such as that differentiating Hits from Misses, produces a transient increase in cortical spiking, but not an increase in Hit rate.

Prolonged choice-related depolarization in cortex

Intracellular recording, recently possible in task-performing animals[19,32,33], reveals the subthreshold membrane potential (V_m) dynamics that govern spiking. To investigate the transformation of thalamic and other synaptic inputs into choice-related spiking, we made intracellular (whole cell) recordings from non-fast-spiking cortical neurons across all layers (n = 22) during our detection task (Fig. 5a; Supplementary Fig. 5). We used intrinsic signal imaging (Methods) to target recordings to the cortical column representing the whisker used to solve the task.

Our whisker stimuli depolarized the membrane potential of nearly all recorded neurons (21 of 22). These V_m responses occurred at short latency (~7 ms on average). We analyzed V_m on Hit, Miss and Correct Rejection trials after removing spikes from the raw V_m traces (Fig. 5b). Depolarization was larger on average for Hits compared with Misses (Fig. 5c). This difference emerged rapidly following stimulus onset (within approximately 30 ms; Fig. 5c; Supplementary Fig. 5b; initial V_m slopes were greater on Hits vs Misses: 0.53 ± 0.08 vs 0.44 ± 0.10 mV/ms; Hit – Miss difference: 0.10 ± 0.03 mV/ms, p = 0.0049) and persisted for the remainder of the trial (Supplementary Fig. 5). The stimulus-evoked change in membrane potential (ΔV_m; Fig. 5c) was larger on Hits compared with Misses (5.7 ± 0.75 vs 4.3 ± 0.72 mV, p < 1e–3, two-tailed sign test, n = 22; Fig. 5d). Approximately 90% (20 of 22) of neurons showed larger ΔV_m on Hit trials. In contrast, we observed no Hit vs Miss difference in pre-stimulus V_m mean or standard deviation (mean: −59.6 ± 1.3 vs −59.1 ± 1.3 mV, p = 0.13; standard deviation: 2.4 ± 0.21 vs 2.5 ± 0.23 mV, p = 0.64; Fig. 5e). Thus, successful

detection is associated with a widespread difference in stimulus-evoked depolarization (see also: [19]).

How well do membrane potential dynamics predict the choice of the mouse on a trial-by-trial basis? We again calculated detect probability, but based on ΔV_m rather than spike rate. The majority of neurons (15 of 22) showed choice-related membrane potential dynamics (DP over evoked window: 0.58 ± 0.03, p = 0.04, two-tailed sign test, n = 22 neurons; 95% confidence interval: [0.52, 0.65]; Fig. 5f). ΔV_m also strongly discriminated stimulus presence vs absence (SP: 0.83 ± 0.03, p < 1e–3, two-tailed sign test; Fig. 5f). Stimulus probability rose above chance level rapidly following stimulus onset (within 8 ms), peaked early (15 ms), and remained above chance level for the remainder of the trial (Fig. 5g; Supplementary Fig. 5). Detect probability rose following stimulus onset (within ~10–12 ms) and persisted above chance level for the remainder of the trial (Fig. 5g; Supplementary Fig. 5).

Comparison of VPM spike rate and cortical V_m on Hits vs Misses showed distinct time courses, with a transient Hit vs Miss difference in VPM and a prolonged difference in V_m (Supplementary Fig. 6). Similarly, detect probabilities calculated separately from VPM spike rate (Fig. 3g) and cortical V_m showed striking differences in dynamics (Fig. 5g). In thalamus, detect probability showed a brief “bump” immediately after stimulus onset, which rapidly disappeared (Fig. 5g). In cortical V_m, detect probability increased more slowly and persisted for the duration of the trial (Fig. 5g). This difference in time course was not explained by convolving the VPM activity with an exponential kernel chosen to simulate the passive membrane time constant of cortical neurons (Supplementary Fig. 6). Moreover, the prolonged Hit vs Miss difference in ΔV_m (Fig. 5c) contrasted sharply with the transient increase in S1 spiking produced by our optogenetic microstimulation in VPM (Fig. 4i,j).

To examine the relationship between choice-related depolarization and choice-related spiking in individual cortical neurons, we obtained spike times from our V_m recordings (Fig. 5h). We calculated detect probability based on spike rate for the same neurons in which we had previously calculated detect probability based on V_m (Fig. 5i,j). Across the neurons that spiked during our recordings (19 of 22; our methods allowed us to sample rarely-spiking neurons[31]), mean spike rate detect probability was 0.54 ± 0.02 (p = 0.21, two-tailed sign test of DP = 0.5). Spike rate detect probability and stimulus probability both rose following stimulus onset in a subset of neurons (Fig. 5i; time series for the top third of neurons ranked by DP, corresponding to 7 purple symbols in Fig. 5j; 2 neurons had individually significant spike rate DP > 0.5 by permutation test). Comparison of detect probabilities calculated from spike rate and membrane potential did not reveal a clear relationship (Fig. 5j, left; note that the precise time courses of spike rate and subthreshold detect probabilities can differ due to such factors as spike rate adaptation). Nearly all neurons (21 of 22) discriminated the stimulus condition (present vs absent) in their membrane potential (SP > 0.5), but only a subset did so in their spiking (Fig. 5j, right).

Top-down feedback of choice-related activity to S1

We observed a prolonged choice-related depolarization in most S1 neurons (Fig. 5c,d). Choice-related differences in the rapid, feedforward response to whisker stimulation were

too transient to explain this prolonged choice-related depolarization (Figs. 3, 4; Supplementary Figs. 4,6). The late phase of this cortical response may be relevant for the perceptual decision[19]. To investigate sources of choice-related activity other than feedforward[17] drive (cf. [8]), we used two-photon calcium imaging during behavior to monitor top-down axons[34] projecting from secondary somatosensory (S2) cortex to layer 1 of S1 (Fig. 6a,b). Inputs to layer 1 are thought to provide state-dependent modulation of cortical activity[35].

Whisker stimulation produced activity-dependent[26,34] increases in axonal fluorescence (Fig. 6c,d). These top-down inputs showed enhanced responses on Hits compared with Misses (Fig. 6d), prior to the earliest reaction times (Fig. 6e; 0.027 ± 0.003 vs 0.015 ± 0.003 $\Delta F/F0$, p = 0.0078, K-S test, n = 167 axons from 4 mice). Activity in these axons predicted choice on a trial-by-trial basis (Fig. 6f; detect probability, mean: 0.529 ± 0.005; 95% confidence interval: [0.516, 0.534]; median: 0.528). Thus, S1 receives top-down input from S2 that predicts perceptual choice.

V_m stimulus sensitivity predicts choice-related spiking

Not all sensory cortex neurons show choice-related activity[1]. This neuron-to-neuron variability is poorly understood[3,36]. We analyzed our intracellular recordings in more detail to understand what determines whether a neuron converts a widespread choice-related depolarization (Fig. 5c,d) into choice-related spiking.

First, we asked whether three biophysical quantities that affect neuronal excitability could explain which neurons showed choice-related spiking: (1) V_{spike}, the membrane potential at which a spike is initiated; (2) V_{rest}, resting membrane potential; (3) $V_{rest} - V_{spike}$, which sets the amplitude of depolarization necessary to cause a spike. Surprisingly, none of these simple measures of excitability correlated with spike rate detect probability (Fig. 7a).

Next, for each neuron we calculated the whisker stimulation reversal potential (V_{rev}; Fig. 7b)[18–21]. V_{rev}, is the membrane potential toward which a stimulus drives a neuron. If V_{rev} exceeds spike threshold ($V_{rev} > V_{spike}$), the stimulus will drive the neuron to spike. V_{rev} is thus an intracellular measure of stimulus sensitivity[18–20].

As expected, there was a strong correlation between spike rate stimulus probability (a measure of stimulus sensitivity) and $V_{rev} - V_{spike}$ (Fig. 7c, right; $R^2 = 0.6$, p = 0.001). Remarkably, we found that $V_{rev} - V_{spike}$ also strongly predicted spike rate detect probability (Fig. 7c, left; $R^2 = 0.6$, p = 0.001; Supplementary Fig. 7; the effect was mainly due to V_{rev}: $R^2 = 0.44$, p = 0.0096). The subthreshold stimulus sensitivity of a neuron, therefore, accounts for its spike rate detect probability.

If spike rate detect probability and stimulus probability are both determined by subthreshold stimulus sensitivity ($V_{rev} - V_{spike}$), they should be correlated (cf. [1,6,10,12,37,38]). To test this prediction, we calculated detect probability and stimulus probability for 1,746 layer 2/3 neurons from our two-photon imaging dataset. Detect probability and stimulus probability were weakly but significantly correlated (Fig. 7d; n = 1,746 neurons in 6 mice; $R^2 = 0.14$, p < 1e–3; Supplementary Fig. 8).

Together, these results show that the stimulus sensitivity of a neuron determines whether it will convert a widespread choice-related depolarization into choice-related spiking.

Discussion

We traced perceptual choice-related variability in spike rate across the early somatosensory system of mice, from primary afferents to cortex. Choice-related variability in spike rate was absent in the primary afferents, and was weak and transient in thalamus. In contrast, choice-related activity was prominent in cortex. The transient choice-related differences in VPM thalamic spiking could not account for the prolonged choice-related activity in cortex. Top-down axons projecting from secondary to primary somatosensory cortex signaled upcoming choice. Within single cortical neurons, an intracellular measure of stimulus sensitivity governed the mapping of a widespread choice-related depolarization into spiking.

Microneurography studies in humans[16] (and a recent study in monkeys: [39]) have demonstrated the power of combining psychophysics with single-unit recording from primary afferents. We have adapted this approach to the mouse, a genetically tractable organism, by recording from primary afferents during a perceptual task. In humans, receptor type and location shape the ability to perceive spikes from primary afferents[16]. Our approach will permit monitoring and manipulating genetically defined classes of receptor neuron to assay their impact on perceptual behavior.

What are the contributions of feedforward, feedback and local circuit processing to cortical choice-related activity? Here we found a significant but transient detect probability in thalamic relay neurons of VPM, which provide the main feedforward drive to whisker S1. Though choice (and detect) probability has been studied almost entirely in cortex, a previous study reported significant choice probabilities in subcortical structures[6]. The brief time course of detect probability in VPM, however, argues against the possibility that cortical choice-related activity is simply inherited in a passive feedforward manner from VPM. Moreover, pairing optogenetic stimulation in VPM with S1 recordings showed that a transient difference in feedforward thalamic spiking could not by itself generate a sustained difference in S1 activity (e.g. via local processing within the cortical column).

We observed choice-related activity in a feedback circuit comprising axons projecting from S2 to S1. This supports a prior finding of top-down contributions to choice probability in monkey visual cortex[8], and is consistent with the stronger choice-related activity in S2 compared with S1 of monkeys[14]. Additional long-range inputs to S1 may also play a role, for instance neuromodulatory[40] axons, projections from the higher-order posteromedial thalamic nucleus[41], or top-down projections from other motor-sensory areas[34,42,43].

We found that mouse S1 neurons showed robust choice-related activity. In contrast, during a tactile detection task in monkeys, choice probability exceeded chance levels only in areas downstream of S1[14,44]. Because of the greater number and specialization of somatosensory areas in primates, features of neural activity present in mouse S1 may first emerge at downstream areas in primate. The extent to which different sensory brain areas show choice-related activity, and the role of task features, is an active topic of investigation[9,11,12,44,45].

We applied ideal observer analysis based on spike rate (over tens to hundreds of milliseconds) to recordings from primary afferents, thalamus, and cortex. We did this to understand variability in cortical spike rate, which has been widely observed to predict choice[1,2,4,6–11,13,14]. However, the relevant features of neural activity could differ across areas[30], and even in S1 may encompass features other than spike rate[24]. Indeed, we found that Hits and Misses differed slightly in a measure of thalamic synchrony[29,30]. Future work will compare alternative approaches to decode choice based on multiple features of neural activity. In addition, computational work suggests that choice probability is shaped by patterns of inter-neuronal correlations, which may differ across perceptual tasks[3,7,36,46,47]. Future work is required to understand whether our findings during tactile detection generalize to other tasks, such as the discrimination of similar stimuli.

We found no clear effect of pre-stimulus neural activity on detection in primary afferents, thalamus, or cortex. However, we quantified pre-stimulus activity using only simple measures. More sophisticated analyses, such as those based on population decoding[48,49] or precise knowledge of network oscillations[24], might reveal an influence of pre-stimulus brain state on perceptual choice. In addition, we aimed to reduce variation in pre-stimulus behavioral state by alerting the mice to the time of possible stimulus arrival on every trial (via an auditory cue). This may have encouraged heightened levels of vigilance and/or affected neuromodulatory[40,50] systems that can alter neural variability.

Neurons with higher choice probability tend to be more sensitive to the stimulus (e.g. have lower “neurometric” thresholds)[1,6,10,12,37]. This is intriguing because it suggests that more sensitive neurons contribute more to perceptual decisions. However, computational[46] and theoretical work[38,47] has shown that multiple factors, including both read-out strategies[47] and inter-neuronal correlations, can shape choice probability[3,7,36]. Here we provide a mechanistic view of the correlation between choice probability and stimulus sensitivity at the level of membrane potential in single cortical neurons. Specifically, we show that the subthreshold stimulus sensitivity of a neuron explains both its spike rate stimulus sensitivity and its detect probability.

Our results trace the emergence of choice-related activity as sensory information is transformed from primary afferents to cortex, and within individual cortical neurons. Choice-related variability in neural activity emerged largely at the cortical level. Choice-related activity was relatively weak along the rapid feedforward pathway, but prominent in a major feedback pathway, to S1 cortex. A widespread, subthreshold choice signal was transformed into spiking in a subset of cortical neurons according to their stimulus sensitivities. Our work offers a key step toward mechanistic dissection of correlations between sensory cortex activity and perceptual choice.

Methods

All procedures were in accordance with protocols approved by the Johns Hopkins University Animal Care and Use Committee. Data analyses were conducted in MATLAB. Schematics of brain coronal sections (Figs. 3–6, Supplementary Figs. 2–4,8) were adapted from The Allen Mouse Brain Atlas (http://atlas.brain-map.org).

Mice

Mice were C57BL/6NHsd (Harlan) and were adults (>8 weeks) except where specified. We report 22 whole cell recordings from S1 (barrel) cortex in 17 males with ages ranging from 7–12 weeks; 17 extracellular recordings in VPM during behavior from 4 males; 48 total recordings with optogenetic VPM stimulation from mice obtained by crossing Scnn1a-Tg3-Cre[51] (Jackson Labs: 009613; B6;C3-Tg(Scnn1a-cre)3Aibs/J) mice with Ai32[52] (Jackson Labs: 012569; B6;129S-Gt(ROSA)$^{26Sortm32(CAG-COP4*H134R/EYFP)Hze}$/J) mice on a mixed background: 12 from VPM in 3 females, 21 from S1 of awake mice in 2 males, and 15 from S1 during behavior in 1 male and 2 females; 17 extracellular recordings in trigeminal ganglion (TG) during behavior from 6 males; neuronal stimulus-response curves from 16 loose-seal cell-attached recordings in S1 in 2 females, 15 extracellular recordings in VPM in 2 females, 9 extracellular recordings in TG in 2 males; two-photon calcium imaging data from L2/3 neurons in 6 males; axon imaging data from 4 males; muscimol silencing experiments in 2 males; optogenetic silencing experiments in 2 females obtained by crossing PV-IRES-Cre[53](Jackson Labs: 008069; B6;129P2-Pvalb$^{tm1(cre)Arbr}$/J) with Ai32 mice on a mixed background; behavior experiments from 6 adult C57BL/6NHsd males and 1 adult male obtained by crossing TH-Cre (Jackson Labs: 008601) with Ai32 mice on a mixed background. Mice were housed in a vivarium with reverse light-dark cycle (12 hours each phase). Experiments occurred during the dark phase. Mice were house in groups of up to 5 prior to the start of water restriction, after which mice were housed singly.

Surgery for electrophysiology

Titanium headposts were implanted for head fixation[22]. Briefly, mice were anesthesized (1–2% isoflurane in O_2; Surgivet) and mounted in a stereotaxic apparatus (David Kopf Instruments). Body temperature was maintained with a thermal blanket (Harvard Apparatus). Scalp and periosteum over the dorsal surface of the skull were removed. The skull surface was scored with a dental drill and the headpost was affixed using cyanoacrylate adhesive (Krazy Glue) followed by dental acrylic (Jet Repair Acrylic). An opening (“well”) in the headpost over the left hemisphere was covered with silicone elastomer (Kwik-Cast, WPI) followed by a thin layer of dental acrylic.

Intrinsic signal imaging

After recovery from headpost surgery (> 24 hours), mice were anesthetized with light isoflurane (0.5–1%) and chlorprothixene (0.02 ml of 0.36 mg/ml, IM). Intrinsic signal imaging (ISI) was performed as described[22]. In most cases, the target whisker was right C2. In rare cases C2 was missing at the time of ISI, and D2 or C3 was substituted. ISI was performed through the skull, typically with the skull covered by a thin layer of cyanoacrylate adhesive, and in some cases also by a thin layer of clear nail polish (Electron Microscopy Sciences) to reduce glare.

Behavioral task

Behavioral apparatus was controlled by BControl software (C. Brody, Princeton University). For 7–10 days prior to training, mice received 1 ml/day of water. On training days, mice were weighed before and after each training session to determine water consumed. Mice

were allowed to perform the task until sated. Additional water was given if mice consumed < 0.3 ml. In the first 1–2 sessions, mice received a drop of water (~6 μl) each time the tongue contacted a "lickport" tube placed near their snouts. In subsequent sessions, mice were operantly conditioned to lick at the lickport in response to a passive whisker deflection. The target whisker (on the right side of the face for S1 and VPM recordings, on the left side for TG recordings) was threaded into a glass pipette attached to a piezo actuator (Piezo Systems), with ~3–5 mm at the base exposed. In S1 experiments, all whiskers except the target whisker were trimmed to near the base. In VPM and TG experiments, all whiskers were shortened. For training, on Go trials, the whisker was deflected for 1.5 s with a 40 Hz sinusoidal deflection (rostral to caudal, peak angular speed ~800 deg/s). A "Hit" trial occurred when mice licked the lickport within a response window, and a drop of water was delivered (~6 μl). The response window was defined as 0.2–2 s after onset of whisker stimulation. The initial 0.2 s after stimulus onset was a "grace period" in which licks had no consequence. On Go trials, if mice did not lick within the 1.8 s response window, it was scored as a "Miss" trial, and no reward or punishment was delivered. Go trials were randomly mixed with NoGo trials, in which the whisker was not deflected. No more than 3 consecutive trials of the same type were allowed. On NoGo trials, if mice licked within the response window, it was scored as a "False Alarm", and mice were punished with a 3–5 s timeout. If mice licked during the timeout, an additional timeout was triggered. A "Correct Rejection" occurred when mice withheld licking during the response window. Correct Rejections were not rewarded. After performance reached >65% of trials correct, the duration of the whisker stimulus was shortened to 0.5 s. After performance reached >65% correct with the shorter stimulus, a 0.1 s auditory cue (8 kHz tone, ~80 dB SPL) was introduced starting 1 s preceding stimulus onset. During all sessions, ambient white noise (cut off at 40 kHz, ~80 dB SPL) was played through a separate speaker to mask any other potential auditory cues associated with movement of the piezo stimulator. Mice were considered trained when performance reached >70% correct for at least two consecutive days (0.5 s, ~800 deg/s stimulus). Typically, mice were trained one session per day for 1–2 weeks to reach this criterion. The behavioral task for two-photon imaging sessions used a 20 Hz (0.5 s) sinusoidal whisker deflection instead of 40 Hz. One additional step was implemented for the mice trained for VPM and TG recordings. In later training sessions, the target whisker was selected arbitrarily among the large caudal vibrissae to ensure that mice could generalize the task to other whiskers.

For the single-vs-three whisker psychometric curve experiments (Fig. 1d), 3 mice were trained initially with single whisker deflections (rostral-caudal; peak angular speed ~800 deg/s). Later, a second piezo stimulator was introduced and mice were tested using deflections of either a single whisker (C3) or three whiskers (C1, C2, C3 deflected simultaneously), with four different angular speeds ranging from ~300–1,200 deg/s. In total, there were 9 trial types (8 Go types: single and three whisker deflection, each with 4 speeds, and 1 NoGo type). Thus, each session had 8 hit rates and 1 false alarm rate. Trials were selected randomly from among these 9 types, subject to the constraint that NoGo trials were 50% of all trials. Performance with stronger, multi-whisker stimulation (gray plot symbol in Fig. 1d) was assayed in a separate experiment after training on the single-whisker task. The piezo stimulator was positioned in a vertical configuration such that the glass pipette was in

contact with multiple (3–5) whiskers. The auditory cue was omitted. On Go trials, multiple whiskers were deflected for 1.5 s at 40 Hz (rostral-caudal, ~2,200 deg/s).

Mice sometimes began a behavior session with impulsive licks (False Alarm rate > 0.4 and/or Miss rate < 0.1), or, in cases where mice had to wait to start the task after a prolonged search for an electrophysiological recording, a low Hit rate (< 0.16). These blocks of initial trials were excluded from analysis (49 ± 29, mean ± SD).

We focused our analyses on Hit, Miss and Correct Rejection trials for the following reasons: (a) False Alarm trials in mice can be due in part to impulsive licking; (b) we had few False Alarm trials to work with in our dataset (after excluding any trials at the beginning of the session that reflected impulsive licking). Analysis of this limited dataset confirmed that responses on False Alarm trials were larger than those on Correct Rejections (Supplementary Fig. 9).

Trigeminal ganglion recording

Under isoflurane (1–2%), a craniotomy of 1 mm by 2 mm (medial-lateral, anterior-posterior) was made over the left hemisphere, centered at 1 mm posterior to bregma and 1 mm lateral to midline. Mice were transferred to the behavior/recording apparatus and lightly anesthetized (0.5–1.5% isoflurane). A tungsten microelectrode (1.0 or 2.0 MΩ nominal, WPI) was advanced vertically through the brain at the speed of 50–100 μm/s until reaching the depth of 5.5 mm, then slowly advanced (~10 μm/s) while manually stimulating ipsilateral whiskers to find whisker responsive neurons in TG. Evoked spikes were monitored via oscilloscope (Tektronix) and audio monitor (A-M Systems). The craniotomy was typically covered with 2% agarose (Sigma-Aldrich) in “cortex buffer” (in mM: 125 NaCl, 5 KCl, 10 Glucose, 10 HEPES, 2 $CaCl_2$, 2 $MgSO_4$, pH 7.4) to reduce brain movement. After successfully identifying whisker responses in TG, the penetration site was marked as a reference for future recordings.

During subsequent behavioral sessions, mice were first lightly anesthetized (0.5–1.5% isoflurane). A tungsten microelectrode (1.0 or 2.0 MΩ nominal, WPI) was advanced to the previously mapped region. After locating a single unit and determining its single whisker receptive field, the whisker was inserted into the whisker stimulator in its “resting position”. Test stimuli identical to those used during the behavioral task were applied with the whisker stimulator. Neurons that could be manually stimulated but could not be made to spike with the rostral-caudal whisker stimulation were not recorded. If piezo stimulation evoked spikes, isoflurane was turned off, and the animal was allowed to recover for 15–30 min. After recovery, the behavioral task was initiated. Electrophysiological signals were amplified 1,000×, filtered at 300–3,000 Hz (DAM80, WPI) and acquired at 20 kHz with Ephus (www.ephus.org). During the recording, electrophysiological signals were monitored and, if necessary, the electrode was slightly adjusted to maintain recording quality. After each session, the headpost well was covered with silicone elastomer and a thin layer of dental acrylic. We found that recording quality remained acceptable over tens of electrode penetrations across 3–4 days.

TG recording: data preprocessing

Voltage recordings were filtered between 300–3,000 Hz in software. A threshold for spike detection was manually set for each trial. Spike sorting to obtain single units was performed in MClust-4.0 (AD Redish et al.). Trials with large movement artifacts were rejected, as determined by large amplitude voltage fluctuations occurring prior to stimulus onset. In all, we obtained 45 ± 21 (mean ± SD) trials per single unit for analysis.

VPM recording

Under isoflurane (1–2%), a craniotomy (~1 mm diameter) was made over the left hemisphere, centered at 1.8 mm posterior to bregma, 1.5 mm lateral to midline[54]. Under light isoflurane (0.5–1.5%), a tungsten microelectrode (1.0 MΩ nominal impedance, Parylene-coated, WPI) was advanced vertically through the brain (MP-225, Sutter) at a speed of 50–100 μm/s until reaching the depth of 2.5 mm, then slowly advanced at ~10 μm/s. Contralateral whiskers were manually deflected after advancing each 30–50 μm. Evoked spikes were monitored using an oscilloscope (Tektronix) and audio monitor (AM Systems). We used the somatotopic organization of VPM (including the whiskers, other facial regions, teeth and microvibrissae), and the presence of other structures (lateral geniculate nucleus) as a guide during mapping. If no whisker-evoked activity was identified by a depth of 4 mm, the electrode was withdrawn and reentered at a neighboring site. This procedure was repeated until clear whisker-evoked responses could be identified around a depth of 3 mm. The craniotomy was typically covered with agarose (2% in cortex buffer) to reduce brain movement. This mapping process took 1–4 hours. After successfully locating a recording site, a map of brain surface vasculature was manually drawn and used to locate penetration sites for future recordings.

During subsequent behavioral sessions, mice were placed in the behavior apparatus and lightly anesthetized (0.5–1.5% isoflurane). A tungsten microelectrode (1–2 MΩ nominal, WPI) was advanced to the previously mapped region. The electrode was then slightly moved along its tract while whiskers were manually deflected in order to identify the “principal” whisker producing the strongest response. At this point, the principal whisker was inserted into the whisker stimulator, isoflurane was turned off, and the mouse was allowed to recover from anesthesia. During recovery, test stimuli identical to those used during the behavioral task were applied and evoked spiking was monitored to detect any movement-related signal degradation (decrease in spike height). In these cases, careful advancement or withdraw of the electrode usually recovered the signal. Otherwise, a new recording was sought. After 15–30 minutes (during which time the mouse fully recovered from anesthesia), the behavioral task was initiated. Electrophysiological signals were amplified 1,000× or 10,000× and filtered 300–3,000 Hz (DAM80, WPI) and acquired at 20 kHz with Ephus. During the recording, electrophysiological signals were monitored and if necessary the electrode was slightly adjusted to maintain recording quality. If quality (amplitude of evoked spikes) degraded too severely to be recovered within 2–3 Go trials, behavioral trials were paused until high-quality multiunits were regained. After each session, the headpost well was covered with silicone elastomer and a thin layer of dental acrylic. We found that recording quality remained acceptable over tens of electrode penetrations across >1 week. To aid recording site identification, a microelectrode coated with DiI (Life Technologies) and

lowered into the brain following the same trajectory used for recording. The brain was later perfused (PBS flush followed by 4% PFA), post-fixed overnight (4% PFA), sectioned coronally at 100 μm thickness on a vibratome (Microm), and processed for cytochrome oxidase staining. Brightfield and fluorescent images (BX-41 microscope, Olympus) were acquired (QImaging) and DiI tracts were used to verify VPM targeting (Supplementary Fig. 3).

VPM recording: data preprocessing

Voltage recordings were filtered between 300–3,000 Hz in software. Traces were inspected visually and included for analysis if spike height was >4–5 times the standard deviation (SD) of baseline noise. The threshold for spike detection was set manually to be at least 4–5 SD of baseline noise, and was constant across all trials in a recording session. Detected spikes were not sorted and were presumably multiunits. Trials with large movement artifacts were rejected, as determined by large amplitude voltage fluctuations occurring prior to stimulus onset. In all, we obtained 63 ± 26 (mean ± SD) trials per multiunit recording for analysis.

VPM recording: interpretation of multi-unit activity

Detect probability calculations for VPM were based on multi-unit (~2–5 neurons) rather than single-unit activity as in our primary afferent and cortical recordings (but see Supplementary 3e–g for results from 7 single units). Our VPM detect probability calculations may therefore differ from the detect probabilities expressed by single neurons. This would not change our conclusion that VPM shows significant but highly transient choice-related activity.

VPM optogenetic stimulation with recordings

Optrodes were implanted in Scnn1a-Tg3-Cre;Ai32 mice. Optrodes were made by gluing a tungsten microelectrode (2.0 MΩ nominal impedance, Parylene-coated, WPI) to a multimode optic fiber (105 μm core diameter, 0.22 NA, Thorlabs), with the microelectrode tip extending ~100 μm beyond the tip of optic fiber. VPM was located as described above using a normal (non-optrode) tungsten microelectrode. This microelectrode was then withdrawn and an optrode was used to probe the target site and surrounding area to relocate VPM. The optrode was coupled to a 470 nm LED (M470F1, Thorlabs) with high-power driver (LEDD1B, Thorlabs). The maximal output from the optrode was 170–230 μW before implantation. Targeting was considered successful when (a) clear spiking was driven by deflection of a principal whisker (usually C2), and (b) photostimulation (50–100 ms pulses at full power) yielded spikes with similar amplitude as those evoked by principal whisker stimulation.

To record VPM activity evoked by photostimulation with and without whisker stimulation in awake mice, isoflurane was withdrawn and the principal whisker was inserted into the piezo stimulator. While recording with the optrode in VPM, three types of stimuli were delivered on separate trials: (1) whisker alone, (2) whisker plus “weak” photostimulation (40–60 μW, 1ms), or (3) whisker plus “strong” photostimulation (170–230 μW, 1ms). The light pulse was delivered at either 0, 3 or 4 ms following the onset of the whisker stimulus (rostral-caudal, peak angular speed ~1,200 deg/s). A second light pulse was given 1.5 s after the first

pulse to determine the effect of light stimulation alone. Based on calculations[55] (www.optogenetics.org/calc) of light intensity vs distance from fiber tip, we estimate an excitation volume of roughly 1–3 thalamic barreloids. Data preprocessing was as described above for VPM.

To record S1 responses to VPM stimulation in awake (Supplementary Fig. 4) or task-performing (Fig. 4g–m) mice, the exposed brain was first covered with agarose (2% in cortex buffer) and dental cement was used to secure the optrode in place. The skull over barrel cortex was kept clear of dental cement. The next day, a craniotomy (~200 μm diameter) was made over the cortical barrel column (identified using ISI) corresponding to the principal whisker of the VPM optrode recording (identified using whisker stimulation and photostimulation). Glass pipettes and recording procedures were identical to those described below for whole cell recording steps prior to break-in, except that pipettes were filled with cortex buffer and seal resistance was ~20–50 MΩ. For recordings (current clamp mode, I = 0) in awake non-performing mice, trials of the three types used in VPM recordings were delivered with equal probability. For recordings in performing mice, the three types of Go trials (whisker alone, whisker + weak photostimulation, whisker + strong photostimulation) comprised 60–70% of all trials. The remaining trials were of three NoGo types: no stimulus, weak photostimulation alone, strong photostimulation alone). The light pulse (1 ms duration) was delivered 4 ms following the onset time of the whisker stimulus (awake mice: rostral-caudal, peak angular speed ~1,200 deg/s; task-performing mice: rostral-caudal, peak angular speed ~800 deg/s). Silent cells[31] which spiked very sparsely or did not respond to whisker stimulation were avoided during the process of establishing the recording.

Whole cell recording

Under light isoflurane (1–1.5%), the skull above the C2 column, previously localized via intrinsic signal imaging, was thinned with a dental drill. A craniotomy (~200 μm diameter) was made by removing a small piece of the thinned bone with a tungsten needle (Fine Science Tools). The mouse was transferred to the behavior apparatus and allowed to recover from anesthesia. Borosilicate glass pipettes (1.5 mm OD, 0.86 mm ID; Harvard Apparatus) were pulled (P-97, Sutter) to have a long shank and were 4–7 MΩ when filled with solution containing (in mM): 135 potassium gluconate, 4 KCl, 10 sodium phosphocreatine, 4 ATP magnesium salt, 0.3 GTP sodium salt hydrate, 10 HEPES, 3 mg/ml biocytin (pH 7.3 with KOH). Electrophysiological signals (Multiclamp 700B, Molecular Devices) were filtered at 10 kHz and acquired at 20 kHz using Ephus. Voltage clamp mode was used to search for neurons. Square wave voltage pulses (50 ms, −5 mV, 5 Hz) were applied to the electrode tip to monitor resistance. Positive pressure of ~3 psi was applied as the pipette tip approached the cortical surface at an angle of 27 deg relative to vertical. A sudden change of pipette resistance indicated contact. Micromanipulator (MP-225, Sutter) depth reading of the cortical surface was recorded, and the pipette was quickly retracted by ~200 μm. Agarose (2%) in cortex buffer was applied to cover the craniotomy. The pipette was then quickly advanced through the dura (if necessary) to ~200 μm below the surface (~100 μm/s). Pipette pressure was then reduced to 0.3–0.5 psi, and the pipette was advanced slowly (~10 μm/s) to search for neurons. When an abrupt increase in pipette resistance (30–50%) was observed,

positive pressure was released. Sometimes negative pressure was applied (< 0.2 psi) to facilitate seal formation. Before break-in, pipette capacitance and offset were compensated. Break-in was performed when resistance was >1GΩ and stable. Break-in was accomplished by applying a slow ramp of negative pressure (up to 1 psi) repetitively. Brief voltage pulses (Multiclamp "zap" function) were occasionally used to assist. After successful break-in, the recording mode was switched to current clamp (I = 0), any negative pressure was released, and the behavioral session was initiated. Traces of raw membrane potential were acquired for each behavioral trial, synchronized via triggers from the behavior control software. Liquid junction potential was not corrected. The recording was terminated when the recorded cell was lost, when membrane potential became depolarized above −40 mV, or when the mouse stopped performing the task. Typically each mouse could be recorded from for one session per day over 2–3 days, with a typical yield of one cell per animal.

Whole cell recording: recording rejection criteria

Recorded trials were rejected for analysis if resting V_m was above −45 mV, or resting V_m increased by more than ~10 mV from the value measured in the first trial. A test pulse (50 pA current injection, 0.2 s) was delivered at the end of each trial. Mean total resistance to ground (R_{total} = series resistance + neuronal input resistance) was calculated using the voltage change caused by the test pulse averaged across all trials. Voltage change was calculated by subtracting mean V_m over a baseline window (0.5–0.1 s prior to test pulse onset) from mean V_m in a window during the test pulse (0.05–0.15 s after onset). Recording sessions were excluded from further analysis if R_{total} exceeded 300 MΩ. R_{total} for accepted recordings (n = 22) was 201.9 ± 44.3 MΩ (mean ± SD). In all, we obtained 37 ± 22 (mean ± SD) trials per neuron for analysis.

Whole cell recording: spike removal and resting potential estimate

To remove spikes, V_m was first median filtered and then smoothed using a 4–10 ms (depending on spike width) moving average. Resting membrane potential (V_{rest}) was calculated as mean V_m in a window 0.1–0.5 s after trial onset (~0.1 s before auditory cue) across all accepted trials.

Whole cell recording: spike detection and spike threshold estimate

Spikes were detected offline using a threshold (10–30 mV) applied to bandpass filtered (100–3,000 Hz) V_m. Spike threshold, V_{spike}, was estimated using a 2 ms window of V_m ending at the time of the action potential peak. Within this window, V_{spike} was estimated as the V_m at which the maximum of the second derivative of V_m occurred.

Whole cell recording: PSP slope estimate

PSP slopes were estimated by fitting a line to V_m over an approximately 10 ms window containing the most linear and steepest V_m within the first 30 ms after stimulus onset. In most cases, the slope was estimated within the first 20 ms.

Whole cell recording: reversal potential

The evoked PSP (V_m following the stimulus) was estimated in a 10–20 ms window starting typically 10–20 ms after stimulus onset, and was plotted against pre-stimulus V_m (mean over a 20 ms window preceding stimulus onset). A line was fitted to these x,y pairs using linear regression. V_{rev} was the fitted value of pre-stimulus V_m (extrapolated past the last × value in some cases) at which the evoked PSP is 0. We attempted to calculate V_{rev} in the 19 of 22 neurons in which action potentials occurred (where we could determine V_{spike}). Out of these, 5 of 19 showed poor linear fits (R^2: 0.15 ± 0.11 [mean ± SD]), which can occur due to insufficient numbers of trials such that observations do not span an adequate range of pre-stimulus V_m. Linear fits were good (R^2: 0.69 ± 0.19 [mean ± SD]) and allowed estimation of V_{rev} in the remaining 14 of 19 neurons. V_{rev} did not differ between Hit and Miss trials (−54.6 ± 4.9 vs −53.9 ± 8.0 mV [mean ± SD], p = 0.49).

Two-photon calcium imaging of layer 2/3 somata

A circular craniotomy was made over the left barrel cortex (2.5 mm diameter; center relative to bregma: lateral, 3.5 mm; posterior, 1.3 mm) of P40–50 mice. The dura was left intact. GCaMP6s[26] was expressed under the human synapsin-1 promoter following infection with recombinant adeno-associated virus (serotype 2/1, Syn.GCaMP6s.WPRE.SV40, University of Pennsylvania Gene Therapy Program Vector Core). Injections were made at 4–6 sites within the craniotomy (30–50 nl per site; depth, 250–300 μm; ~1 nl per second). After virus injection, the craniotomy was covered with an imaging window made by gluing together two pieces of microscope cover glass[48]. The smaller piece (Fisher; number 2 thickness) was fitted into the craniotomy and the larger piece (number 1.5 thickness) was glued to the bone surrounding the craniotomy[48]. To localize a barrel column within the cranial window, intrinsic signal imaging was performed through the window 1 week after surgery. All whiskers on the right side of the snout except the relevant one (a row C whisker) were trimmed after the intrinsic signal imaging. Mice were then water restricted for 2 weeks prior to training. Imaging was started 3–5 weeks after surgery. To minimize active whisking[56], botulinum toxin A (BOTOX, Allergan) was prepared in PBS at 1 ‘mouse units’ (MU)/μl, and 0.5 MU was injected to the right whisker pad of trained mice using a 1 μl syringe (Hamilton). Mice fully recovered from the toxin treatment after ~7 days.

Images were acquired on a custom two-photon microscope (http://openwiki.janelia.org/wiki/display/shareddesigns/MIMMS) equipped with a resonant scanning module (Thorlabs), GaAsP photomultiplier tube (Hamamatsu) and a 16× 0.8 NA microscope objective (Nikon). GCaMP6s was excited at 1000 nm (40–60 mW at specimen) with a Ti-Sapphire laser (Chameleon Ultra II, Coherent). Imaging fields were restricted to areas where GCaMP6s expression overlapped with the desired barrel columns. The field of view was 760 μm × 790 μm (440 × 512 pixels; pixel size, 1.72 μm × 1.55 μm). Images were acquired continuously at 15 Hz using ScanImage 4.1/4.2 (www.scanimage.org). A movie, corresponding to a single trial, consisted of 65 image frames.

Two-photon calcium imaging of S2→S1 axons

Adeno-associated virus (serotype 2/1, Syn.GCaMP6s.WPRE.SV40) was injected into S2 (relative to bregma: lateral, 4.3 mm; posterior, 1 mm) at 2 depths (250 μm and 350 μm; 30–

40 nl each; ~1 nl per second), and covered with a cranial window. Intrinsic signal imaging was performed through the window. GCaMP6s expression was examined under a wide-field fluorescence microscope, and mice showing excessive cell body fluorescence outside the ISI-localized S2 region were excluded. Imaging planes were from layer 1 of S1 (70–100 μm from pial surface). The field of view was 100 μm × 108 μm (440 × 512 pixels; pixel size, 0.23 μm × 0.21 μm). Images were acquired continuously at 30 Hz using ScanImage 4.2. A movie, corresponding to a single trial, consisted of 140 image frames.

Two-photon calcium imaging of layer 2/3 somata: data analysis

A line-by-line correction algorithm was used to correct for brain motion[48]. For each behavioral trial, we used five consecutive frames with a minimum of luminance changes to generate an average reference image. Each line was registered to the reference image by maximizing the line-by-line Pearson correlation. Regions of interest (ROIs) corresponding to individual neurons were manually selected with the help of maximum intensity and standard deviation projections across movie frames. For each ROI, the time series of raw fluorescence was estimated by averaging all pixels within the ROI. Neuropil signal surrounding each ROI was estimated by averaging all pixels, excluding those from neighboring ROIs, within a 2 pixel-wide ring that starts at 2 pixels away from the border of the ROI. This neuropil signal was subtracted from the raw fluorescence time series to yield the corrected fluorescence time series: $F(t) = F_{raw}(t) - r \times F_{neuropil}(t)$, with r = 0.7[26,57]. $\Delta F/F_0$ was calculated from this corrected fluorescence signal as $(F-F_0)/F_0$, where F_0 was the mean F over 4 baseline frames immediately preceding the time of stimulus onset for each trial. Evoked $\Delta F/F_0$ was calculated as the mean $\Delta F/F_0$ over 3 frames following the stimulus onset time and before the answer lick (~100–300 ms after stimulus onset). For presentation in Figs. 1f and 6c only, we subtracted a baseline comprising the mean $\Delta F/F_0$ of the 10 frames preceding the stimulus.

Two-photon calcium imaging of S2→S1 axons: data analysis

To distinguish ROIs that belong to the same axon from those that belong to different axons, we used a correlation-based method (adapted from: [34]) to build clusters of highly correlated ROIs. Only responsive ROIs were included in the clustering and subsequent analysis. To determine whether a ROI was "responsive," an evoked $\Delta F/F_0$ value was calculated using the mean F over 8 frames immediately preceding the stimulus onset time as F_0, and the mean F over 20 frames immediately following the stimulus onset time as the post-stimulus response. A Wilcoxon signed rank test (for samples with absolute value skew <0.6) or a sign test (absolute value skew >0.6) was performed on these evoked $\Delta F/F_0$ values. If the resulting p-value was <0.01, the neuron was considered "responsive." Analysis procedures subsequent to clustering were as described above for L2/3 somata, except that neuropil subtraction was not performed, F_0 was calculated using 8 baseline frames (due to 30 Hz rather than 15 Hz imaging), and evoked $\Delta F/F_0$ was calculated as the mean $\Delta F/F_0$ over 5 frames following the stimulus onset time (from ~117 to 283 ms after stimulus onset). The $\Delta F/F_0$ for each putative "axon" was calculated as the mean $\Delta F/F_0$ of all ROIs within a cluster.

Optogenetic and pharmacological silencing

PV-IRES-Cre;Ai32 mice were implanted with a clear skull cap[23]. Light from a 473 nm laser (MBL-III-473-100, Ultralasers) was passed through an acousto-optic modulator (MTS110-

A3-VIS, QuantaTech), focused into a multimode optical fiber, recollimated and directed onto the C2 column (targeted using ISI). The beam at the skull had an approximately Gaussian profile with FWHM of 600 μm. Photostimulation was randomly delivered on 25–35% of all trials. Photostimulation comprised a train of 5 ms pulses at 100 Hz delivered from −300 ms to +2,200 ms relative to the time of whisker stimulus onset. Average power at the brain surface was ~3 mW. A visual masking flash (2 ms pulses at 10 Hz) was delivered for the duration of every trial via a 470 nm LED (7007-PB000-D, LEDdynamics) placed near the eyes.

Muscimol hydrobromide (Sigma-Aldrich) was dissolved in cortex buffer at 5 ug/ul and stored at −20 deg C. For injection, mice were anesthetized with isoflurane and kept on a thermal blanket. A craniotomy was made as described for whole cell recordings. Muscimol was injected into the C2 column (identified by intrinsic signal imaging) in different sessions as follows: 100 nl at 500 μm (n = 2 sessions total in 2 mice), 50 nl at 350 and 700 μm (total 100 nl, n = 1). V1 injection was performed at 3 mm posterior to bregma and 2 mm lateral to midline with 150 nl at 350 and 700 μm (total 300 nl, n = 2 sessions total in 2 mice) and 300 nl at 500 μm (n = 1). Injection was performed at the speed of ~1 nl/s. After injection, the pipette was left in place for 3 min. Mice were allowed 1.5–3 hours to recover before initiating the behavioral session.

Stimulus-response curves for TG, VPM and S1 in awake mice

Recordings were obtained as described above for TG, VPM and S1, except that S1 recordings were made with cortex-buffer filled pipettes in loose-seal cell-attached[31] rather than whole cell mode. Whisker stimuli (0.5 s, rostral-caudal sinusoidal deflections) of four different amplitudes (~300, 600, 900, 1,200 deg/s peak angular speeds) were randomly delivered with equal probability. Windows and procedures for calculating evoked responses were identical to those used for TG, VPM and S1 recordings acquired during task performance (described below).

Licking artifact removal and licking trial exclusion

We used an electrical method of detecting tongue contact with the lickport. Contact could cause brief artifacts in electrophysiology traces. In V_m analysis, this artifact was already removed by median filtering and smoothing (see above). For spike rate analysis (whole cell and extracellular recordings), the raw voltage samples from −3.75 to +3.75 ms, centered at the lick, were replaced by the mean value over −7.5 to −3.75 ms and +3.75 to +7.5 ms relative to the lick. Licking artifacts had negligible impact on our analyses because: (a) we limited analyses to periods prior to the earliest reaction times (occurring ~0.2 s post stimulus onset), and (b) trials with “premature” licks occurring close to stimulus onset (in a window from −0.583 s to + 0.12 s relative to the time of possible stimulus onset for electrophysiology, and −0.5 s to +0.12 s for calcium imaging) were excluded from subsequent analysis.

Elimination of whisking artifacts

Multiple experimental strategies and results ensure that periods of spontaneous whisking did not significantly impact our results. First, as described above for the two-photon imaging of

S1 neurons, we used BOTOX to eliminate the ability of mice to whisk. We obtained similar results in separate experiments without BOTOX (not shown). Second, we observed that periods of whisking in our trained mice are nearly always accompanied by movement artifacts in our metal microelectrode recordings. Epochs with movement artifacts were excluded as described above. Third, although whisker movements would cause a difference in neural activity, we observed no differences in pre-stimulus baseline activity in any of our recordings (Fig. 2–5). Fourth, any differences in mechanical input that affect brain activity must first cause spiking in the mechanoreceptive primary afferent neurons. We recorded from these primary afferents and observed no differences between Hits and Misses (Fig. 2).

Anesthesia and task performance

As detailed above, TG, VPM and S1 whole cell recording sessions involved use of anesthesia prior to task performance. Our two-photon sessions, however, did not involve anesthesia. The behavioral performance levels obtained in these anesthesia-free sessions (73 ± 3% correct, n = 10 sessions) did not differ from those obtained in sessions involving anesthesia (74 ± 8% correct, n = 56 sessions; p = 0.78, Wilcoxon rank sum test). Thus, anesthesia did not have a noticeable impact on performance.

Data analysis: windows for measurement of baseline and evoked activity

For all electrophysiological recordings, pre-stimulus baseline activity was calculated using a 200 ms window ending 3 ms before stimulus onset. Post-stimulus activity was calculated in a 100 ms window starting 5 ms after stimulus onset for V_m and a 100 ms window starting 7 ms after stimulus onset for spike rate in whole cell recordings, a 10 ms window starting 5 ms after stimulus onset for VPM “peak” response calculation, a 100 ms window starting 15 ms after stimulus onset to calculate VPM “after peak” response, and a 27 ms window starting 2 ms after stimulus onset for TG recordings. The window length of 27 ms was chosen to include the first two peaks of the TG evoked response. Because some TG neurons we recorded were direction selective (not shown), the first two peaks capture the initial response of all neurons. Our conclusions are similar if we include only the first peak. For VPM recordings combined with photostimulation, we used the same “peak” and “after peak” windows as described above for VPM. For cell-attached recordings in S1 combined with VPM photostimulation, post-stimulus activity was calculated in a 30 ms window starting 5 ms after stimulus onset for “peak” response, and a 100 ms window starting 35 ms after stimulus onset for “after peak” response. For VPM and S1, evoked AP rate (or V_m) was defined as the difference in AP rate (or V_m) between the post- and pre-stimulus windows. Because baseline TG spike rates were extremely low (medians for Hit and Miss trials: 0.77 and 0.62 Hz, respectively) compared with rates during the stimulus (Hit and Miss medians: 76.6 and 62.7 Hz), evoked AP rate was calculated simply as the AP rate during the post-stimulus window. For TG and S1, results were similar across a range of post-stimulus window sizes (Supplementary Fig. 10).

ROC analysis

We used receiver operating characteristic (ROC) analysis to calculate “detect probability” (mathematically identical to “choice probability”[1], but typically renamed in the context of detection tasks) and “stimulus probability.” For detect probability calculation, Go trials were

split into Hits and Misses. A decision variable (DV) was assigned for each trial based on the neural response. Detect probability was then calculated (using MATLAB 'perfcurve') as the area under the ROC curve for discrimination based on DV. Stimulus probability was calculated using the same method, except that trials were split into Go and NoGo rather than Hits and Misses. For V_m analyses, the DV was ΔV_m. For spike rate analyses the DV was evoked AP rate (defined previously). For two-photon calcium imaging, the DV was evoked $\Delta F/F_0$ (defined previously). Detect probability and stimulus probability time series were calculated in a 5 ms moving window with 1 ms step size.

Statistics

Mice of appropriate genotypes were assigned to experimental groups arbitrarily, without randomization or blinding. A summary of experimental groups is given in Supplementary Table 1. No statistical methods were used to predetermine sample sizes. Data are reported as mean ± standard error of the mean unless otherwise noted. Statistical tests were by two-tailed Wilcoxon signed rank unless otherwise noted (MATLAB 'signrank'). Assumptions of the Wilcoxon signed rank test were verified by quantifying symmetry of the distribution of sample differences about its median. For samples failing this assumption (absolute value skewness > 0.6), we instead used the sign test (MATLAB 'signtest').

Supplementary Material

Refer to Web version on PubMed Central for supplementary material.

Acknowledgments

We thank V. Jayaraman, R. Kerr, D. Kim, L. Looger, K. Svoboda and the HHMI Janelia Farm GENIE Project for GCaMP6. We thank Rohit Gummi for technical assistance; Simon Peron for MATLAB software; Jeremiah Cohen for discussions and help with optrode construction; Terry Shelley for instrument fabrication. We thank Jeremiah Cohen, Genki Minamisawa, Woodrow Shew, Karel Svoboda and Shan Yu for comments on the manuscript. This work was supported by the Whitehall Foundation, Klingenstein Fund, and NIH (R01NS089652, P30NS050274).

References

1. Britten KH, Newsome WT, Shadlen MN, Celebrini S, Movshon JA. A relationship between behavioral choice and the visual responses of neurons in macaque MT. Vis Neurosci. 1996; 13:87–100. [PubMed: 8730992]
2. Celebrini S, Newsome WT. Neuronal and psychophysical sensitivity to motion signals in extrastriate area MST of the macaque monkey. J Neurosci. 1994; 14:4109–4124. [PubMed: 8027765]
3. Nienborg H, Cohen MR, Cumming BG. Decision-related activity in sensory neurons: correlations among neurons and with behavior. Annu Rev Neurosci. 2012; 35:463–483. [PubMed: 22483043]
4. Cook EP, Maunsell JH. Dynamics of neuronal responses in macaque MT and VIP during motion detection. Nat Neurosci. 2002; 5:985–994. [PubMed: 12244324]
5. Bosking WH, Maunsell JH. Effects of stimulus direction on the correlation between behavior and single units in area MT during a motion detection task. J Neurosci. 2011; 31:8230–8238. [PubMed: 21632944]
6. Liu S, Gu Y, DeAngelis GC, Angelaki DE. Choice-related activity and correlated noise in subcortical vestibular neurons. Nat Neurosci. 2013; 16:89–97. [PubMed: 23178975]
7. Cohen MR, Newsome WT. Estimates of the contribution of single neurons to perception depend on timescale and noise correlation. J Neurosci. 2009; 29:6635–6648. [PubMed: 19458234]

8. Nienborg H, Cumming BG. Decision-related activity in sensory neurons reflects more than a neuron's causal effect. Nature. 2009; 459:89–92. [PubMed: 19270683]
9. Nienborg H, Cumming BG. Macaque V2 neurons, but not V1 neurons, show choice-related activity. J Neurosci. 2006; 26:9567–9578. [PubMed: 16971541]
10. Gu Y, DeAngelis GC, Angelaki DE. A functional link between area MSTd and heading perception based on vestibular signals. Nat Neurosci. 2007; 10:1038–1047. [PubMed: 17618278]
11. Palmer C, Cheng SY, Seidemann E. Linking neuronal and behavioral performance in a reaction-time visual detection task. J Neurosci. 2007; 27:8122–8137. [PubMed: 17652603]
12. Nienborg H, Cumming BG. Decision-related activity in sensory neurons may depend on the columnar architecture of cerebral cortex. J Neurosci. 2014; 34:3579–3585. [PubMed: 24599457]
13. Romo R, Hernandez A, Zainos A, Lemus L, Brody CD. Neuronal correlates of decision-making in secondary somatosensory cortex. Nat Neurosci. 2002; 5:1217–1225. [PubMed: 12368806]
14. de Lafuente V, Romo R. Neural correlate of subjective sensory experience gradually builds up across cortical areas. Proc Natl Acad Sci U S A. 2006; 103:14266–14271. [PubMed: 16924098]
15. Cury KM, Uchida N. Robust odor coding via inhalation-coupled transient activity in the mammalian olfactory bulb. Neuron. 2010; 68:570–585. [PubMed: 21040855]
16. Vallbo, AB.; Johansson, RS. Sensory functions of the skin in primates, with special reference to man. In: Zotterman, Y., editor. proceedings of the international symposium held in Wenner-Gren Center; Stockholm. January 13–15, 1976; Pergamon Press; 1976. p. 185-199.
17. Smolyanskaya A, Haefner RM, Lomber SG, Born RT. A Modality-Specific Feedforward Component of Choice-Related Activity in MT. Neuron. 2015; 87:208–219. [PubMed: 26139374]
18. Crochet S, Poulet JF, Kremer Y, Petersen CC. Synaptic mechanisms underlying sparse coding of active touch. Neuron. 2011; 69:1160–1175. [PubMed: 21435560]
19. Sachidhanandam S, Sreenivasan V, Kyriakatos A, Kremer Y, Petersen CC. Membrane potential correlates of sensory perception in mouse barrel cortex. Nat Neurosci. 2013; 16:1671–1677. [PubMed: 24097038]
20. Mateo C, et al. In vivo optogenetic stimulation of neocortical excitatory neurons drives brain-state-dependent inhibition. Curr Biol. 2011; 21:1593–1602. [PubMed: 21945274]
21. Higley MJ, Contreras D. Nonlinear integration of sensory responses in the rat barrel cortex: an intracellular study in vivo. J Neurosci. 2003; 23:10190–10200. [PubMed: 14614077]
22. O'Connor DH, et al. Neural coding during active somatosensation revealed using illusory touch. Nat Neurosci. 2013; 16:958–965. [PubMed: 23727820]
23. Guo ZV, et al. Flow of Cortical Activity Underlying a Tactile Decision in Mice. Neuron. 2013
24. Siegle JH, Pritchett DL, Moore CI. Gamma-range synchronization of fast-spiking interneurons can enhance detection of tactile stimuli. Nat Neurosci. 2014
25. Ollerenshaw DR, et al. Detection of tactile inputs in the rat vibrissa pathway. J Neurophysiol. 2012; 108:479–490. [PubMed: 22514290]
26. Chen TW, et al. Ultrasensitive fluorescent proteins for imaging neuronal activity. Nature. 2013; 499:295–300. [PubMed: 23868258]
27. Zucker E, Welker WI. Coding of somatic sensory input by vibrissae neurons in the rat's trigeminal ganglion. Brain Res. 1969; 12:138–156. [PubMed: 5802473]
28. Temereanca S, Brown EN, Simons DJ. Rapid changes in thalamic firing synchrony during repetitive whisker stimulation. J Neurosci. 2008; 28:11153–11164. [PubMed: 18971458]
29. Ollerenshaw DR, Zheng HJ, Millard DC, Wang Q, Stanley GB. The adaptive trade-off between detection and discrimination in cortical representations and behavior. Neuron. 2014; 81:1152–1164. [PubMed: 24607233]
30. Wang Q, Webber RM, Stanley GB. Thalamic synchrony and the adaptive gating of information flow to cortex. Nat Neurosci. 2010; 13:1534–1541. [PubMed: 21102447]
31. O'Connor DH, Peron SP, Huber D, Svoboda K. Neural activity in barrel cortex underlying vibrissa-based object localization in mice. Neuron. 2010; 67:1048–1061. [PubMed: 20869600]
32. Harvey CD, Collman F, Dombeck DA, Tank DW. Intracellular dynamics of hippocampal place cells during virtual navigation. Nature. 2009; 461:941–946. [PubMed: 19829374]

33. Domnisoru C, Kinkhabwala AA, Tank DW. Membrane potential dynamics of grid cells. Nature. 2013; 495:199–204. [PubMed: 23395984]
34. Petreanu L, et al. Activity in motor-sensory projections reveals distributed coding in somatosensation. Nature. 2012; 489:299–303. [PubMed: 22922646]
35. Cauller L. Layer I of primary sensory neocortex: where top-down converges upon bottom-up. Behav Brain Res. 1995; 71:163–170. [PubMed: 8747184]
36. Nienborg H, Cumming B. Correlations between the activity of sensory neurons and behavior: how much do they tell us about a neuron's causality? Curr Opin Neurobiol. 2010; 20:376–381. [PubMed: 20545019]
37. Law CT, Gold JI. Neural correlates of perceptual learning in a sensory-motor, but not a sensory, cortical area. Nat Neurosci. 2008; 11:505–513. [PubMed: 18327253]
38. Pitkow X, Liu S, Angelaki DE, DeAngelis GC, Pouget A. How Can Single Sensory Neurons Predict Behavior? Neuron. 2015; 87:411–423. [PubMed: 26182422]
39. Yu XJ, Dickman JD, DeAngelis GC, Angelaki DE. Neuronal thresholds and choice-related activity of otolith afferent fibers during heading perception. Proc Natl Acad Sci U S A. 2015; 112:6467–6472. [PubMed: 25941358]
40. Constantinople CM, Bruno RM. Effects and mechanisms of wakefulness on local cortical networks. Neuron. 2011; 69:1061–1068. [PubMed: 21435553]
41. Gambino F, et al. Sensory-evoked LTP driven by dendritic plateau potentials in vivo. Nature. 2014
42. Lee S, Kruglikov I, Huang ZJ, Fishell G, Rudy B. A disinhibitory circuit mediates motor integration in the somatosensory cortex. Nat Neurosci. 2013; 16:1662–1670. [PubMed: 24097044]
43. Zagha E, Casale AE, Sachdev RN, McGinley MJ, McCormick DA. Motor cortex feedback influences sensory processing by modulating network state. Neuron. 2013; 79:567–578. [PubMed: 23850595]
44. de Lafuente V, Romo R. Neuronal correlates of subjective sensory experience. Nat Neurosci. 2005; 8:1698–1703. [PubMed: 16286929]
45. Vazquez Y, Zainos A, Alvarez M, Salinas E, Romo R. Neural coding and perceptual detection in the primate somatosensory thalamus. Proc Natl Acad Sci U S A. 2012; 109:15006–15011. [PubMed: 22927423]
46. Shadlen MN, Britten KH, Newsome WT, Movshon JA. A computational analysis of the relationship between neuronal and behavioral responses to visual motion. J Neurosci. 1996; 16:1486–1510. [PubMed: 8778300]
47. Haefner RM, Gerwinn S, Macke JH, Bethge M. Inferring decoding strategies from choice probabilities in the presence of correlated variability. Nat Neurosci. 2013; 16:235–242. [PubMed: 23313912]
48. Huber D, et al. Multiple dynamic representations in the motor cortex during sensorimotor learning. Nature. 2012; 484:473–478. [PubMed: 22538608]
49. Safaai H, von Heimendahl M, Sorando JM, Diamond ME, Maravall M. Coordinated population activity underlying texture discrimination in rat barrel cortex. J Neurosci. 2013; 33:5843–5855. [PubMed: 23536096]
50. Pinto L, et al. Fast modulation of visual perception by basal forebrain cholinergic neurons. Nat Neurosci. 2013; 16:1857–1863. [PubMed: 24162654]
51. Madisen L, et al. A robust and high-throughput Cre reporting and characterization system for the whole mouse brain. Nat Neurosci. 2010; 13:133–140. [PubMed: 20023653]
52. Madisen L, et al. A toolbox of Cre-dependent optogenetic transgenic mice for light-induced activation and silencing. Nat Neurosci. 2012; 15:793–802. [PubMed: 22446880]
53. Hippenmeyer S, et al. A developmental switch in the response of DRG neurons to ETS transcription factor signaling. PLoS Biol. 2005; 3:e159. [PubMed: 15836427]
54. Poulet JF, Fernandez LM, Crochet S, Petersen CC. Thalamic control of cortical states. Nat Neurosci. 2012; 15:370–372. [PubMed: 22267163]
55. Yizhar O, Fenno LE, Davidson TJ, Mogri M, Deisseroth K. Optogenetics in neural systems. Neuron. 2011; 71:9–34. [PubMed: 21745635]

56. Landers M, Pytte C, Zeigler HP. Reversible blockade of rodent whisking: Botulinum toxin as a tool for developmental studies. Somatosens Mot Res. 2002; 19:358–363. [PubMed: 12590837]

57. Kerlin AM, Andermann ML, Berezovskii VK, Reid RC. Broadly tuned response properties of diverse inhibitory neuron subtypes in mouse visual cortex. Neuron. 2010; 67:858–871. [PubMed: 20826316]

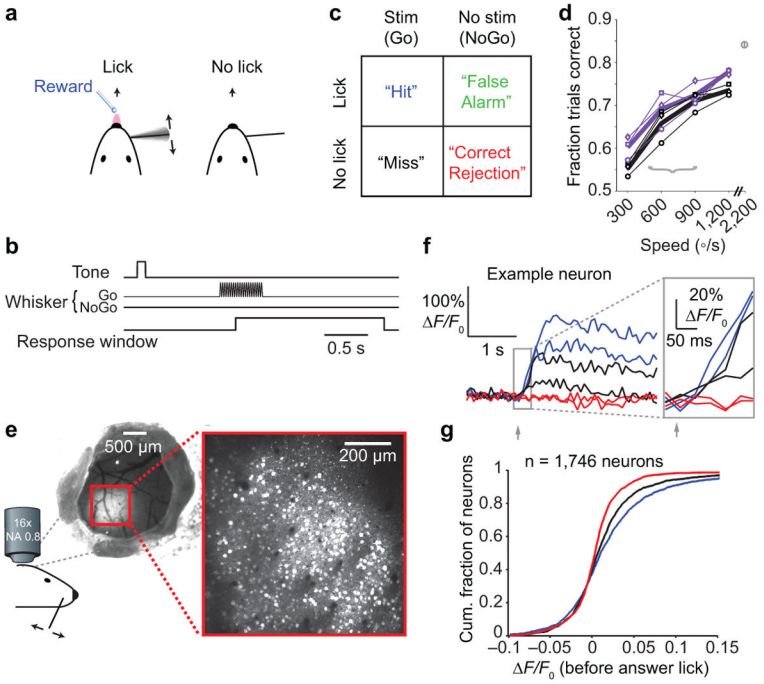

Figure 1. Choice-related activity in mouse primary somatosensory cortex

(a) Tactile detection task based on deflections of a single whisker. (b) Trial structure. A tone alerted mice to the time of possible stimulus onset. On Go trials, the whisker was stimulated with a sinusoidal deflection (0.5 s, 20 or 40 Hz). Mice responded by licking or not licking within a 1.8 s response window. (c) Four trial types are possible, based on the stimulus condition (present/absent) and the response (lick/no lick). (d) Behavioral detection performance varied with deflection speed for a single whisker (thin black lines) and three whiskers deflected simultaneously (thin purple lines). Plot symbols indicate different mice (n = 3). Thick lines show mean performance across mice for deflection of one (black) or three (purple) whiskers. Gray plot symbol at top-right shows performance (n = 2 mice) with strong multi-whisker stimulation. Gray bracket indicates range of speeds used for electrophysiology and imaging experiments. (e) Two-photon calcium imaging of primary somatosensory (S1) cortex during the tactile detection task. Left: cranial window showing region expressing the genetically encoded calcium indicator GCaMP6s. Right: example two-photon image over S1 showing hundreds of individual layer 2/3 neurons (white). (f) Example activity ($\Delta F/F_0$) traces from a single neuron for two Hit (blue), two Miss (black) and two Correct Rejection (red) trials. Inset: early portion of traces, before the earliest behavioral reaction times, used to calculate "evoked" $\Delta F/F_0$. (g) Cumulative histograms showing mean $\Delta F/F_0$ for Hit (blue), Miss (black) and Correct Rejection (red) trials for each neuron (n = 1,746 neurons from 6 mice).

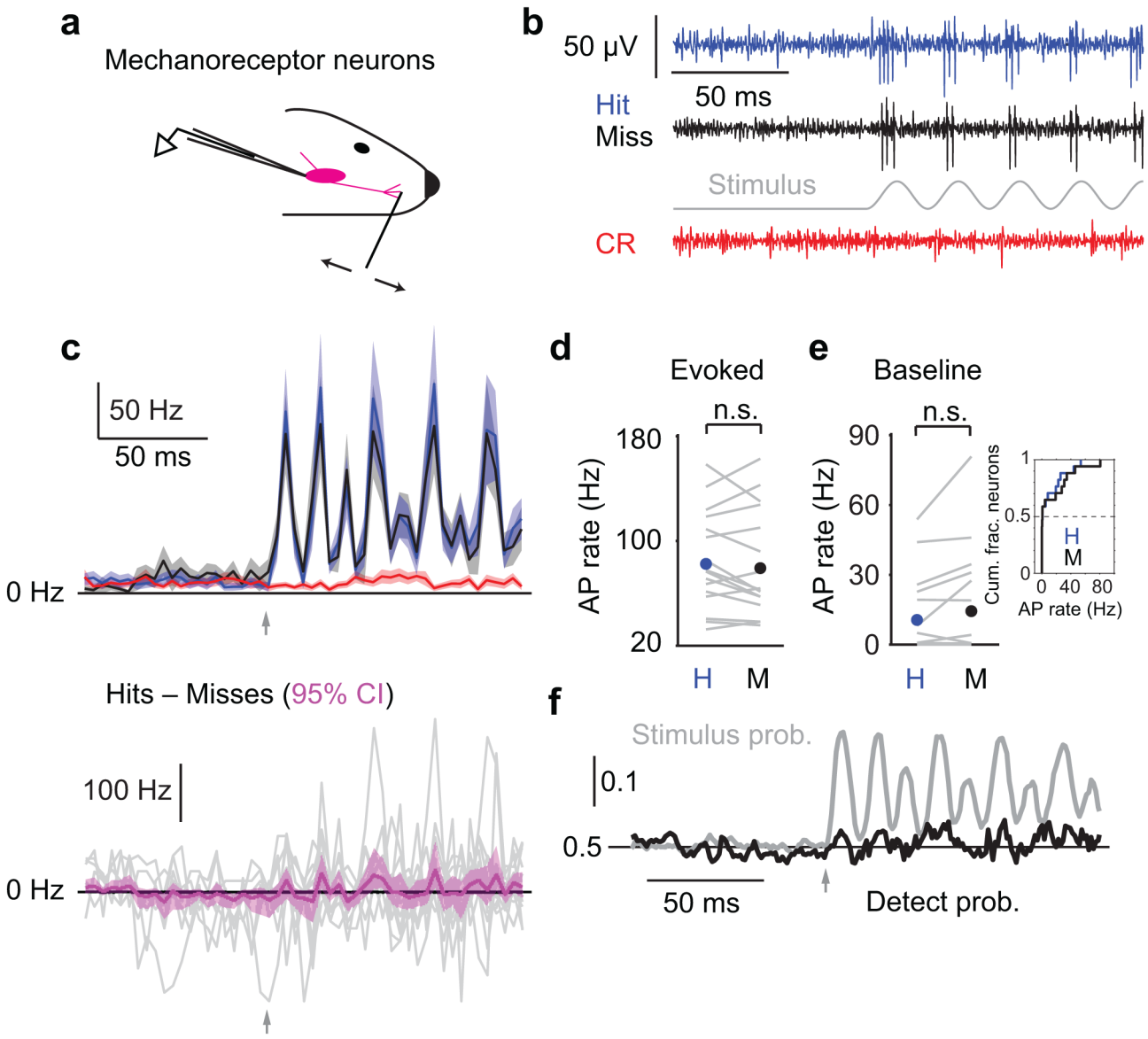

Figure 2. Primary mechanoreceptor afferent neurons do not show choice-related activity

(a) Schematic of extracellular recording from mechanoreceptor neurons in the trigeminal ganglion (TG). (b) Example traces for Hit (blue), Miss (black) and Correct Rejection (red) trials. (c) Top: mean peri-stimulus spike time histograms (PSTHs; 4 ms bins; ± SEM) for n = 17 neurons. Bottom: mean of differences between Hit and Miss PSTHs for each neuron (magenta; mean ± 95% confidence interval). Gray traces: individual neurons. Arrows: stimulus onset. (d) Action potential (AP) rate evoked by the whisker stimulus is similar for Hit (blue circle, mean) and Miss (black circle) trials ($p = 0.38$, $n = 17$). Gray lines: individual neurons. (e) Pre-stimulus AP rate is similar for Hit and Miss trials ($p = 0.55$, two-tailed sign test, $n = 17$). Inset: cumulative histogram of same data. (f) Mean time course of detect probability (black) and stimulus probability (gray) across all TG recordings. Arrow: stimulus onset. n.s., $p > 0.05$;

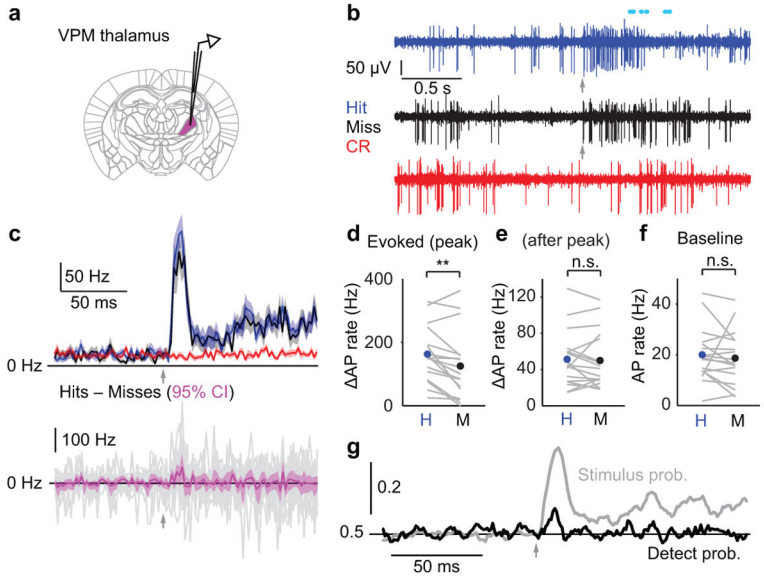

Figure 3. Transient choice-related activity in VPM thalamus

(a) Schematic of extracellular recording in the ventral posteromedial nucleus of thalamus (VPM). (b) Example traces for Hit (blue), Miss (black) and Correct Rejection (red) trials. Arrows: stimulus onset. Cyan circles: licking. (c) Top: mean PSTHs (2 ms bins; ± SEM) for n = 17 recordings. Bottom: mean of differences between Hit and Miss PSTHs for each neuron (magenta; mean ± 95% confidence interval). Gray traces: individual recordings. Arrows: stimulus onset. (d) Evoked AP rate is higher for Hit trials compared with Miss trials during a transient (10 ms) window at the peak of the response ($p = 0.0065$, $n = 17$). (e) Evoked AP rate after the peak of the response showed no difference for Hit and Miss trials ($p = 0.63$, two-tailed sign test, $n = 17$). (f) Pre-stimulus AP rate is similar for Hit and Miss trials ($p = 0.14$, two-tailed sign test, $n = 17$). (g) Mean time course of detect probability (black) and stimulus probability (gray) across all VPM recordings. Arrow: stimulus onset. n.s., $p > 0.05$; **, $p < 0.01$.

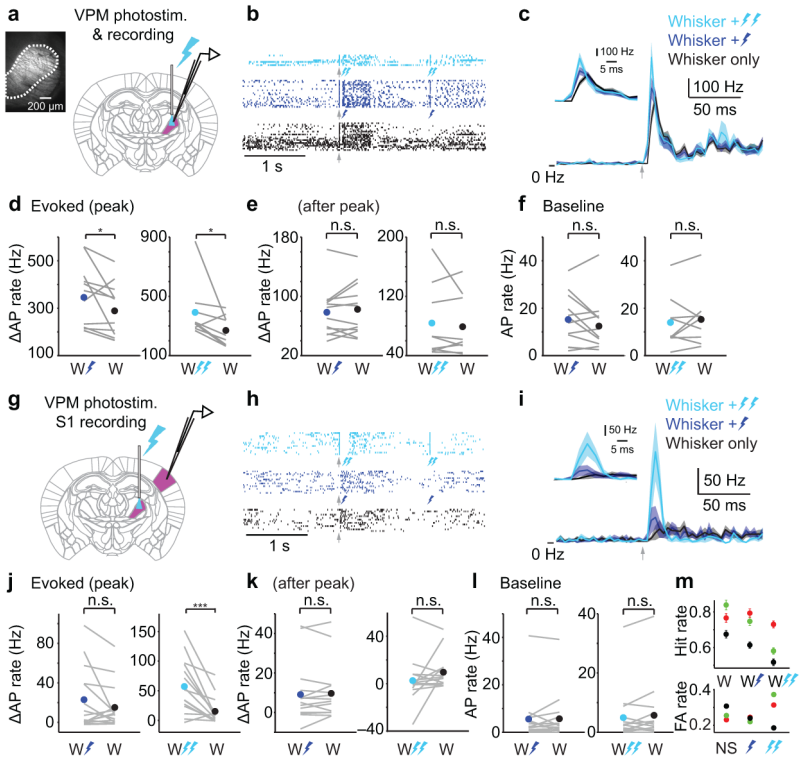

Figure 4. Brief cortical response to transient VPM activity

(a) Schematic of simultaneous optogenetic stimulation and extracellular recording in VPM. Fluorescence image shows channelrhodopsin-2 expression (white) in VPM (dashed outline). (b) Example spike rasters from a VPM recording with whisker stimulation alone (black ticks) or whisker stimulation plus weak (dark blue) or strong (light blue) photostimulation. Arrow: whisker stimulus onset. Dark blue bolt: weak photostimulation. Double light blue bolts: strong photostimulation. Responses to light alone are shown toward the end of the rasters (bolts in the dark blue and light blue rasters). (c) Mean PSTHs (4 ms bins; ± SEM) for whisker-alone (n = 12), whisker plus weak light (n = 12) or whisker plus strong light (n = 9). Inset: zoomed view. Arrow: onset of whisker stimulus followed by light pulse (0–4 ms delay; Methods). (d) Evoked AP rate in a transient (10 ms) window at the peak of the whisker-evoked response is higher for whisker stimulation (“W”) plus photostimulation (dark blue bolt, weak light: p = 0.039, two-tailed sign test, n = 12; double light blue bolts, strong light: p = 0.039, two-tailed sign test, n = 9) compared with whisker stimulation alone. (e) Evoked AP rate after the peak of the whisker-evoked response showed no differences between whisker-alone and whisker plus photostimulation (weak light: p = 0.57, n = 12; strong light: p = 1.0, two-tailed sign test, n = 9). (f) Pre-stimulus AP rate is similar for trials with whisker-alone vs whisker plus photostimulation (weak light: p = 0.34, n = 12; strong light, p = 0.57, n = 9). (g) Schematic of simultaneous optogenetic stimulation in VPM and cell-attached recording in S1. (h) Example spike rasters from an S1 recording. Conventions as in (b). (i) Mean PSTH (4 ms bins; ± SEM) for n = 15 recordings. Inset: zoomed view. Arrow: onset of whisker stimulus followed by light pulse (4 ms delay; Methods). (j) Evoked AP rate for whisker stimulation alone compared with whisker stimulation plus photostimulation (weak light: p = 0.61, two-tailed sign test, n = 15; strong light: p < 1e–3, n

= 15). Whisker-alone data are the same in the left and right panels. (k) Evoked AP rate after the peak of the whisker-evoked response showed no differences between whisker-alone and whisker plus photostimulation (weak light: $p = 0.54$, $n = 15$; strong light: $p = 0.42$, two-tailed sign test, $n = 15$). (l) Pre-stimulus AP rate is similar for trials with whisker-alone vs whisker plus photostimulation (weak light: $p = 0.71$, $n = 15$; strong light: $p = 0.36$, $n = 15$). (m) Behavioral Hit (top) and False Alarm (bottom) rates for three mice (colors) obtained during experiments in (g–l). NS: no stimulus. Symbols show mean performance (± bootstrap SEM) of trials pooled across 5–6 sessions per mouse. n.s., $p > 0.05$; *, $p < 0.05$; ***, $p < 0.001$.

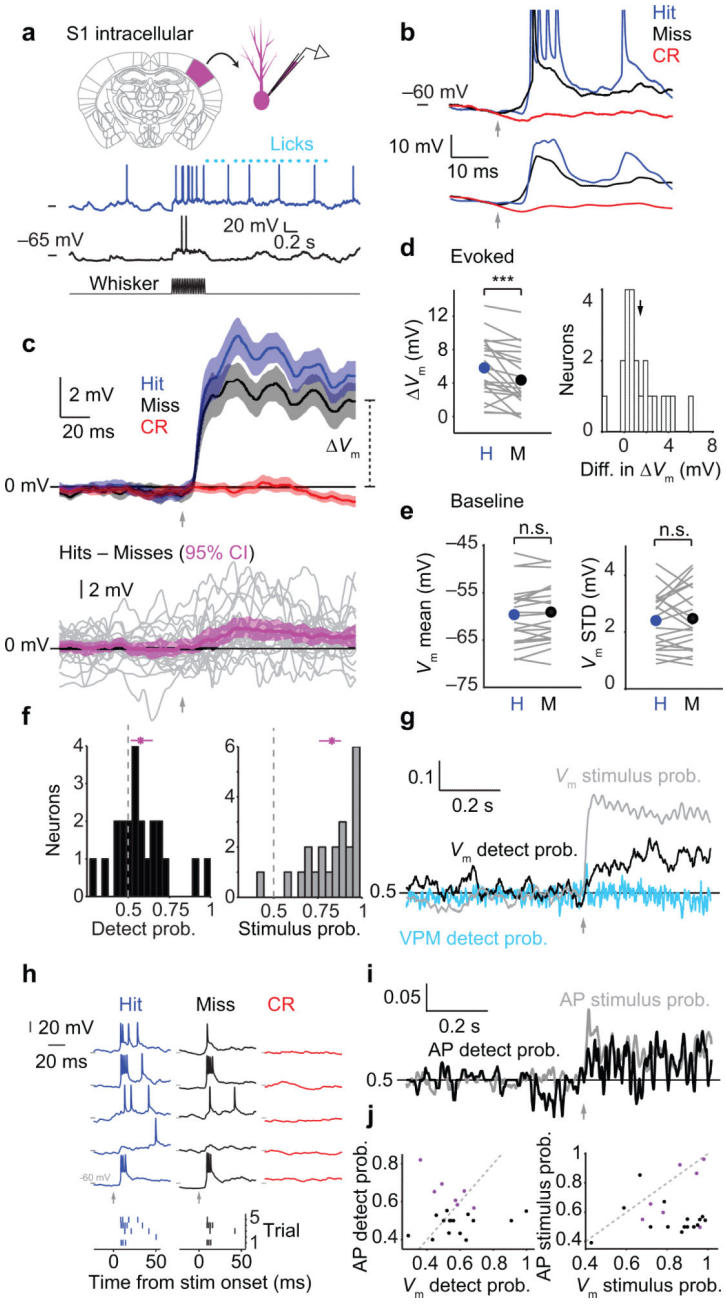

Figure 5. Choice-related membrane potential dynamics in S1 cortex

(a) Top: Schematic of intracellular (whole cell) recording in primary somatosensory (barrel) cortex. Bottom: Example membrane potential (V_m) traces for Hit (blue) and Miss (black) trials. (b) Removing spikes from V_m traces. Top: example raw V_m traces; action potentials (APs; shown truncated) are evident in the Hit and Miss trials. Bottom: the same V_m traces after median filtering and smoothing to eliminate APs. Arrows: stimulus onset for Hit and Miss traces. (c) Top: Mean V_m change after AP removal (± SEM; n = 22 neurons) for Hit (blue), Miss (black) and Correct Rejection (red) trials. Bottom: Mean of differences between mean V_m on Hits and mean V_m on Misses (magenta; mean ± 95% confidence interval; n = 22 neurons). Gray traces: individual recordings. (d) Left: Stimulus-evoked change in

membrane potential (ΔV_m) is larger on Hit trials compared with Miss trials ($p < 1e–3$, two-tailed sign test, $n = 22$). Right: Histogram of the mean difference in ΔV_m between Hits and Misses for each neuron (arrow: mean at 1.4 mV). (e) Pre-stimulus membrane potential dynamics are similar for Hit and Miss trials, both mean V_m ($p = 0.13$, $n = 22$) and standard deviation of V_m ($p = 0.64$). (f) Histograms of detect probability (black) and stimulus probability (gray) computed from ΔV_m. Magenta: means ± 95% confidence intervals. (g) Mean time course of detect probability (black) and stimulus probability (gray) across V_m recordings ($n = 22$). VPM detect probability is shown for comparison (cyan, same data as in Fig. 3g). (h) Extracting action potential times from V_m traces. Top: Example V_m traces from an S1 neuron for Hits, Misses and Correct Rejections. Bottom: action potential rasters obtained from the example traces. (i) Mean time course of detect probability and stimulus probability calculated using action potential times instead of V_m, across the top third of neurons ranked by DP ($n = 7$, corresponding to purple plot symbols in panel (j)). (j) Left: detect probability calculated for each neuron using either action potential rate (y-axis) or evoked change in membrane potential (x-axis). Right: stimulus probability calculated for each neuron using either action potential rate or evoked change in membrane potential. Neurons that did not spike had y-axis values set to 0.5. Purple symbols: neurons included in traces in (i). n.s., $p > 0.05$; ***, $p < 0.001$.

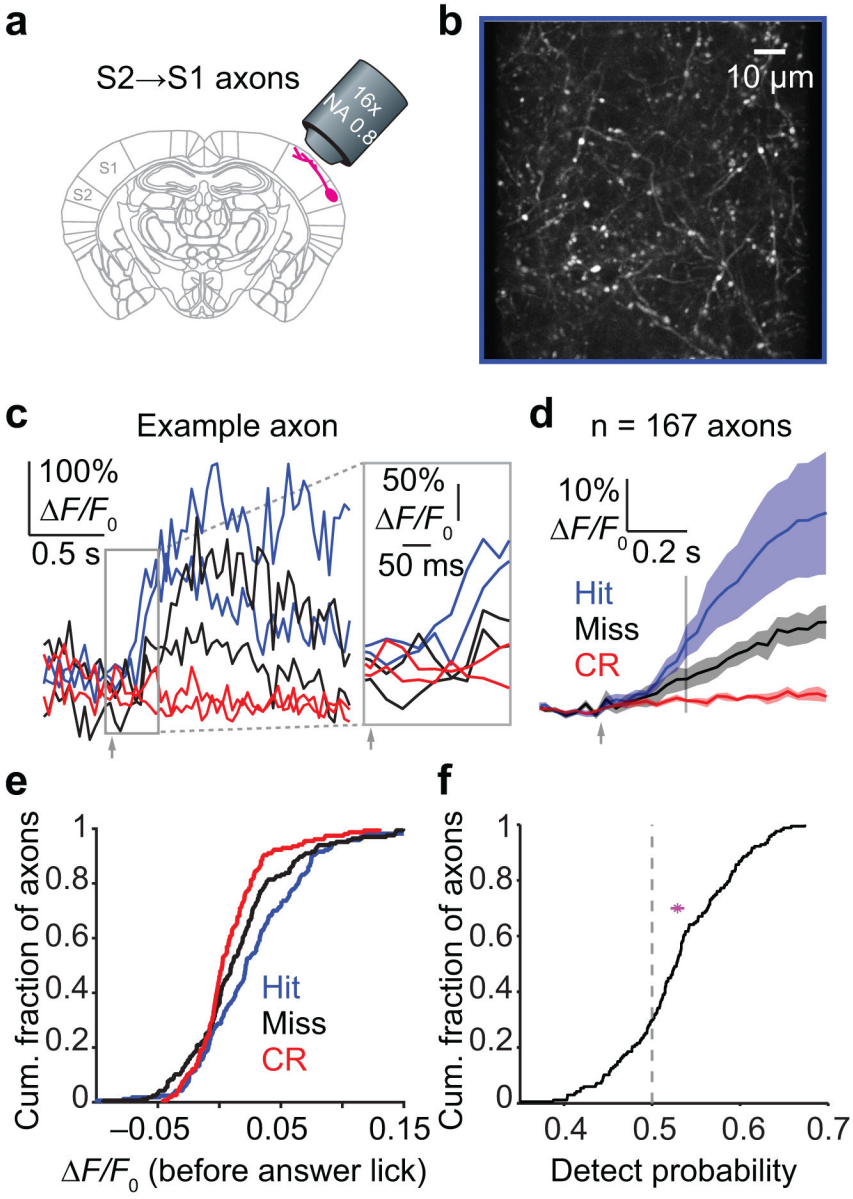

Figure 6. Feedback of choice-related activity from S2 to S1

(a) Schematic of two-photon imaging in S1 from top-down axons projecting from S2 to S1 (S2→S1 axons). (b) Example two-photon image from layer 1 of S1 showing S2→S1 axons (white). (c) Example activity ($\Delta F/F_0$) traces from a single axon for two Hit (blue), two Miss (black) and two Correct Rejection (red) trials. Inset: early portion of traces, before the earliest behavioral reaction times, used to calculate evoked $\Delta F/F_0$. (d) Mean $\Delta F/F_0$ activity time series (± SEM across 4 mice, n = 167 axons total) for each trial type. Vertical line: end of period used for analysis (before the answer lick). (e) Cumulative histograms showing mean $\Delta F/F_0$ for Hit, Miss and Correct Rejection trials for each axon (Hits vs Miss: p = 0.0078, K-S test, n = 167 axons from 4 mice). (f) Detect probability for S2→S1 axons. Dashed line: chance level, 0.5. Magenta: mean ± 95% confidence interval ([0.516, 0.534]; n = 167 axons from 4 mice).

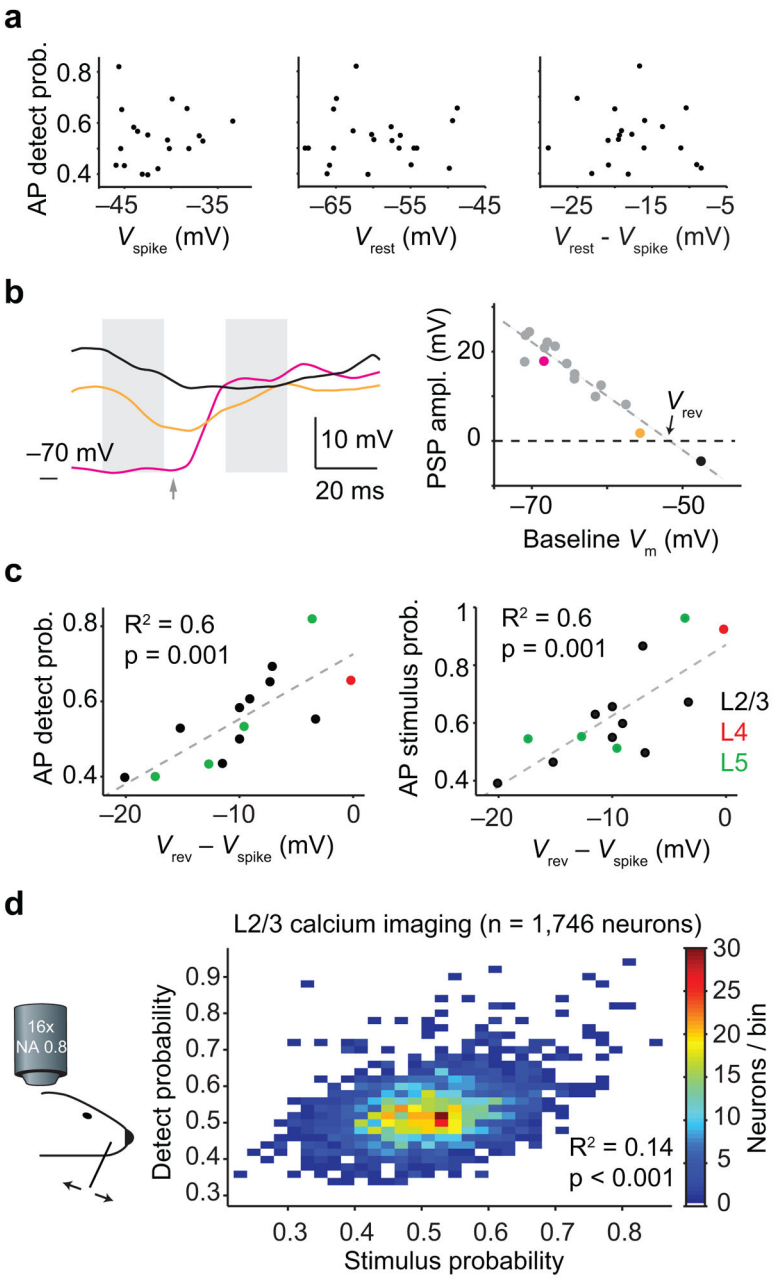

Figure 7. Intracellular stimulus sensitivity predicts choice-related spiking

(a) Biophysical properties related to excitability, including spike threshold (V_{spike}), resting membrane potential (V_{rest}) or their difference, do not explain the magnitude of detect probability. (b) Example reversal potential (V_{rev}) calculation. V_{rev} quantifies the relationship between the amplitude of stimulus-evoked postsynaptic potentials and pre-stimulus membrane potential. Left: example traces of V_m. Gray shading indicates windows used to measure pre-stimulus V_m and evoked PSP (arrow: stimulus onset). Right: PSP amplitude plotted against pre-stimulus V_m shows a linear relationship. Reversal potential, V_{rev}, is defined as the pre-stimulus V_m that produces a zero amplitude PSP. V_{rev} for this neuron is

−51.8 mV. Magenta, yellow and black points correspond to traces in left panel. (c) Spike rate detect probability (left) and stimulus probability (right) are strongly correlated with the difference between reversal potential and spike threshold ($R^2 = 0.6$, $p = 0.001$). Plot symbol color indicates nominal cortical layer (estimated by depth). (d) Detect probability and stimulus probability tend to be higher in the same neurons. Two-dimensional histogram showing correlated detect and stimulus probability ($R^2 = 0.14$, $p < 1e–3$) across populations of S1 layer 2/3 neurons (n = 1,746 neurons from 6 mice).